

Instituto Tecnológico y de Estudios Superiores de Monterrey  
Campus Monterrey  
School of Engineering and Sciences



# **Design and Fabrication of Bioreactors for Tissue Engineering**

*A thesis presented by*

**Ana Valeria González Abrego**

Submitted to the  
School of Engineering and Sciences  
in partial fulfillment of the requirements for the degree of

Master of Science  
In  
Manufacturing Systems

Monterrey Nuevo León, June 15th, 2020

## **Dedication**

This work is dedicated to my family, specially to my parents, Margarita and Fernando, that gave me the opportunity to grow and develop despite the hard work they had to endure to give me what I needed to be who I am today.

To Jorge, that guided me through dark times and made me believe in myself when I needed it the most.

To my friends, that are always there for me when I need them, giving me their unconditional support.

To those professors and tutors that believed in me and gave me the tools I needed to do this work.

## **Acknowledgments**

I would like to start thanking Dr. Ciro Rodriguez for giving me the opportunity to work with him during this time and for supporting and helping me during all this journey. For his time, knowledge, and experience as well as for the resources needed to complete this project.

I am also thanking Dr. David Dean in Ohio State University for giving me a place in his laboratory and his feedback for improving and developing this work.

As well to Tecnológico de Monterrey and Consejo Nacional de Ciencia y Tecnología (CONACYT) for the economic support and the facilities.

Also, thanks to all the other students and mentors that helped me during this process, Dr Mario Alvarez, Dra. Grissel Trujillo de Santiago, and Dra. Raquel Tejeda.

And finally, I would like to thank my parents for helping and encouraging me pursue my research career.

## **Design and Fabrication of Bioreactors for Tissue Engineering**

by

**Ana Valeria González Abrego**

### **Abstract**

Tissue engineering (TE) has provided new techniques to create better tissue models, for study or to solve actual medical problems. Combining TE with design and 3D manufacture techniques can achieve devices that improve actual models. 3D tissue models present a diffusion problem that causes cell death because of the lack of oxygen and nutrients and the concentration of cell waste. Providing flow to the constructs can facilitate perfusion and enhance tissue. To do so, this document presents the designs and prototype development of two bioreactors, with the objective of diminishing necrotic core to create relevant implantable bone tissue and a more realistic breast cancer model. Using DLP and commercially available parts, designs were prototyped and validated.

**LIST OF FIGURES**

Figure 1. TE principles. A) Interaction between scaffold, cells, growth factors and environmental stimuli B) Cell death cause by necrotic core in static culture vs cell growth and correct development due to flow in dynamic culture ..... 1

Figure 2. Difference between indirect and direct perfusion..... 4

Figure 3. Perfusion Bioreactor Development..... 8

Figure 4. Working mechanism of the roller peristaltic pump used in the prototype..... 10

Figure 5. Line components separated view A) Chamber with tubes, scaffold, and scaffold fixations. B) Bubble trap..... 11

Figure 6. CAD design of the scaffold used for particle tracking and mold A) Upper view B) and C) Lateral view D) Strut details E) Aluminum mold used for microfluidics device F) Microscope, bioreactor and microfluidic device layout ..... 13

Figure 7. Static and dynamic experimentation plan ..... 14

Figure 8. CAD of scaffold used for cell culture A) Lateral view B) Front view C) Schoen gyroid strut details ..... 15

Figure 9. Cross section of significant regions in the PPF scaffold. A) Lateral view showing section 1, 2 and 3 used for Calcium Mineralization Assay B) Frontal cut on x axis used in Live/Dean Assay ..... 16

Figure 10. Morphological matrix for bioreactor design with possible combination ..... 18

Figure 11. Bioreactor final prototype..... 19

Figure 12. CFD results. A) Flow trajectory. B) Particle tracking..... 19

Figure 13. Scaffold used for particle tracking A) 3X magnification B) Upper view C) Lateral view D)5X magnification showing strut details E) Scaffold in the microfluidic channel..... 21

Figure 14. A) Screen shot of the tracking particle video showing a velocity probe in b2 region as representation of the division made to obtain data of all the pore, the scale bar represents 100µm B) Average forward flow rate velocity per zone graphic on which each bar represents a region of the pore using the same distribution as in Figure 14A C) Average backward flow rate velocity per zone graphic D) A pie diagram representing the 11 seconds perfusion cycle in which 8 sec. the flow goes forward and 3 sec. it goes backwards E) Bioreactor and microfluidic device connected ..... 21

Figure 15. Fluorescence in RFU representing cell metabolism in Q0, Q11 and Q22 ..... 23

Figure 16. LIVE/DEAD microscopy showing a 1.5X and a 250X representative image of the three study groups at the three time points..... 24

Figure 17. SBC and SSC after ARS in days 5, 10 and 15 ..... 25

Figure 18. SEM images of the seeded scaffolds, A) Cells showing a round morphology at seeding day 2500xB) 3000x C) Spread cells after 7 days of culture 2500x D)3000X (Mishra et al., 2016) E) Scaffold details without cells (Walker, Bodamer, Kleinfehn, et al., 2017)..... 26

Figure 19. Spheroids dynamic and evolvment thru its time in the microfluidics chip ..... 31

Figure 20. Chip design A) Dimensions in all directions B) Exploded view of the entire system ..... 32

Figure 21. Printed chip with mounted scaffold ..... 34

Figure 22. Predicted glucose concentration levels at outlet along 60 days of experimentation and Live/Dead representation during specific time points ..... 35

Figure 23. Key aspects for future successful implantation ..... 37

Figure 24. Tumor-on-chip contributions ..... 38

**LIST OF TABLES**

Table 1. State of the Art in Bone TE Bioreactors ..... 6

Table 2. CFD simulation results..... 20

Table 3. Average Forward and Backward Flow Rate Velocity per zone ..... 22

**TABLE OF CONTENTS**

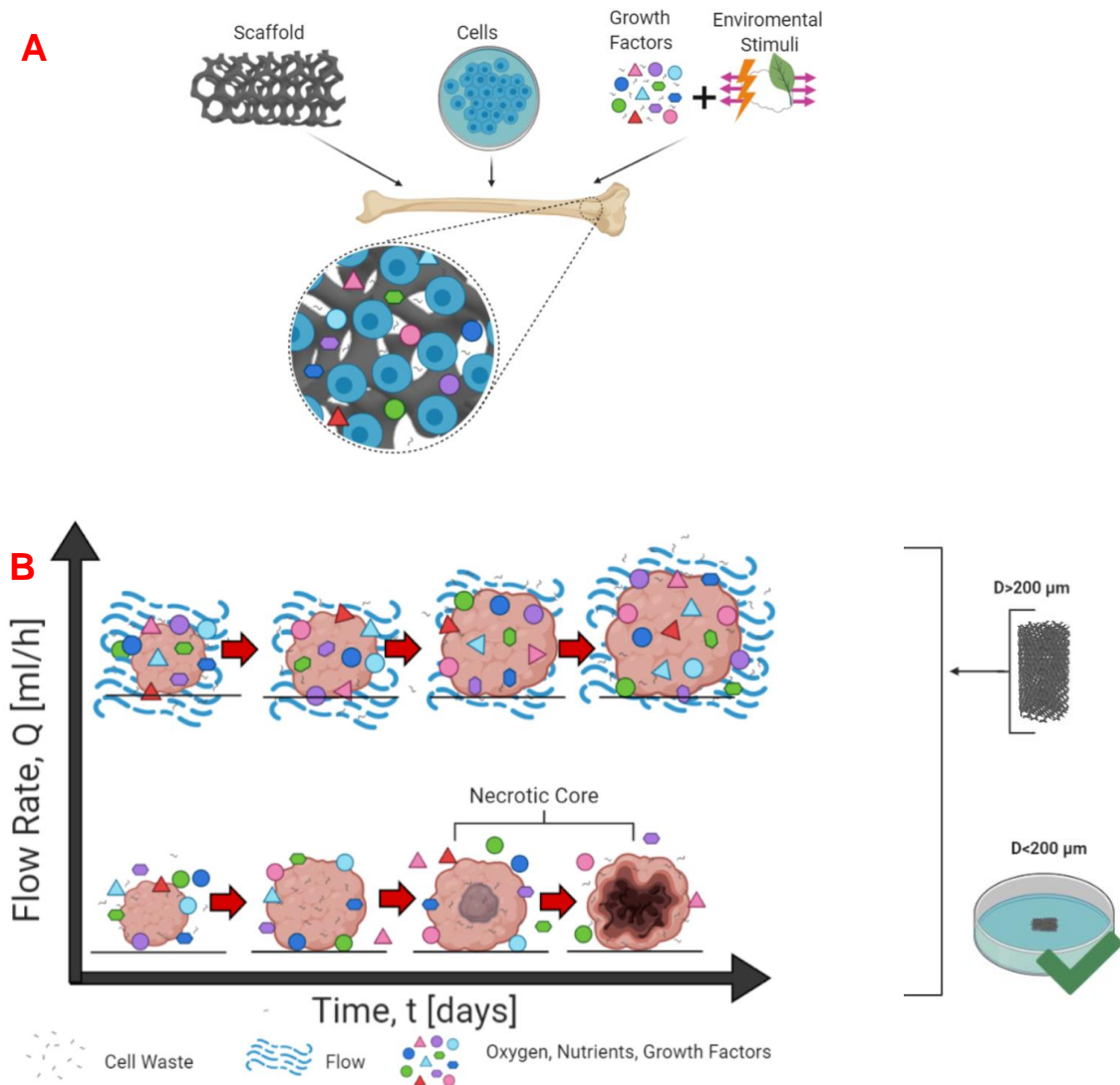
<b>1 INTRODUCTION .....</b>	<b>1</b>
<b>2 PERFUSION BIOREACTOR FOR BONE TISSUE ENGINEERING .....</b>	<b>3</b>
<b>2.1 Introduction .....</b>	<b>3</b>
2.1.1 Bone Implants .....	3
2.1.2 Bioreactor for Bone TE.....	3
2.1.3 Poly- (propylene fumarate) (PPF) as bone TE material .....	4
2.1.4 Related Work .....	4
2.1.5 Objective .....	7
<b>2.2 Materials and Methods .....</b>	<b>8</b>
2.2.1 Design.....	8
<b>2.2.2 Prototyping.....</b>	<b>9</b>
<b>2.2.3 Validation .....</b>	<b>11</b>
2.2.3.1 CFD Analysis.....	11
2.2.3.2 Flow Test with Particle Tracking .....	11
2.2.3.3 Static vs Dynamic Culture .....	14
<b>2.3 Results.....</b>	<b>17</b>
2.3.1 Design.....	18
2.3.2 <i>Prototyping</i> .....	18
2.3.3 Validation .....	19
2.3.3.1 CFD Analysis.....	19
2.3.3.2 Flow Test with Particle Tracking .....	20
<b>2.4 Conclusions and Future Work .....</b>	<b>26</b>
<b>3 TUMOR-IN-A-CHIP / CANCER MODELS .....</b>	<b>27</b>
<b>3.1 Introduction .....</b>	<b>27</b>
3.1.1 4. Related Work .....	28
3.1.2 Objective .....	31
<b>3.2 Materials and Methods .....</b>	<b>31</b>
3.2.1 Chip design and manufacture process.....	31
3.2.2 Tumor-on-chip characterization.....	32
<b>3.3 Results.....</b>	<b>34</b>
3.3.1 Chip design and manufacture process.....	34
3.3.2 Tumor-on-chip characterization.....	34
<b>3.4 Conclusions and Future Work .....</b>	<b>36</b>
<b>4 CONCLUSIONS.....</b>	<b>37</b>
<b>5 REFERENCES .....</b>	<b>39</b>
<b>6 APPENDIX A. PPF CHEMICAL STRUCTURE .....</b>	<b>43</b>
<b>7 APPENDIX B. NECROTIC CORE VISUAL AIDS .....</b>	<b>43</b>



<b>8 APPENDIX C. SKETCHES MADE WITH THE MORPHOLOGICAL MATRIX .....</b>	<b>44</b>
<b>9 APPENDIX D. DG4 MULTI-CHANNEL HEAD ® BY CHONGQING JIEHENG PERISTALTIC PUMP Co., LTD ® .....</b>	<b>45</b>
<b>10 APPENDIX E. ELECTRIC CIRCUIT OF PERISTALTIC PUMP AND ARDUINO CODE.....</b>	<b>46</b>
<b>11 APPENDIX F. DLP PRINTING PROCESS.....</b>	<b>48</b>
<b>12 APPENDIX G. CFD AND PARTICLE TRACKING VIDEO ANALYSIS.....</b>	<b>49</b>
<b>13 APPENDIX H. PURELINK® RNA MINI KIT PROTOCOL .....</b>	<b>50</b>

## 1 Introduction

Nowadays tissue engineering (TE) is considered a major field in research due to the opportunity it provides to satisfy the high demand of living biological tissue that it cannot be successfully attended with organ donors. TE has the ability of developing functional substitutes and new platforms to generate knowledge and solutions in the medical and scientific area. TE is a technique that involves cells, growth factors and biocompatible materials to create tissue for medical uses (Mishra et al., 2016). Cells are incubated in a proper environment in the presence of a scaffold, acting as the support as the extracellular matrix (ECM) gives cells in tissue development in the human body. This phenomenon is illustrated in Figure 1A. TE is done with the intention of proliferating and differentiating cells to have the scaffold full of them for it to be useful when implanted in the injury site (Yeatts & Fisher, 2011).



**Figure 1. TE principles. A) Interaction between scaffold, cells, growth factors and environmental stimuli B) Cell death caused by necrotic core in static culture vs. cell growth and correct development due to flow in dynamic culture**

One of the major concerns in TE laboratories is the transition from 2D to 3D models due to the small size of the diameter ( $<10\text{mm}$ ) and thickness ( $<4\text{mm}$ ) of the tissue that is being made because of the challenge of avoiding a necrotic core (Arano, Sato, Matsuzaka, Ikada, & Yoshinari, 2010). As illustrated in

Figure 1B, diffusion becomes a problem in 3D in-vitro culture when the sample has a distance from its center of about 100-200  $\mu\text{m}$  (Volkmer et al., 2008). The cells in the center of the construct start to die because of the lack of oxygen and high concentration of toxic metabolic waste, spreading cellular death from the center throughout all the scaffold. Creating larger tissue samples requires a new environment that provides perfusion of nutrients, oxygen, and correct disposal of toxic waste. A solution that offers these parameters is a mechanism that delivers a consistent flow, being a bioreactor a viable option (Kanda et al., 2016). The proposed project integrates engineering and biological concepts to create two different mechanism to solve necrotic core difficulties; one is a direct perfusion bioreactor for synthetic bone grafts and the other an organ on a chip device to create a tumoroid with long lifespan.

Being able to build graphs with a significant size to make a difference if implanted and tumor models that are more similar to what we found in the body is a major advance in tissue engineering. The transition of 2D culture to 3D culture has given the opportunity to mimic with more fidelity healthy and diseased tissue, for it to be of use in patients as well as for it to be studied and have a better understanding of its physiology to come up with more efficient treatments. This technique is a step to create a solution that obliterates most of the problems that actual treatments present, such as high infection rates, morbidity, and insufficient donors.

## 2 Perfusion Bioreactor for Bone Tissue Engineering

### 2.1 Introduction

#### 2.1.1 Bone Implants

Regenerative bone material is nowadays a major concern in material research. This is because critical bone defects affect annually .5 million patients representing a cost of more than \$2.5 billion dollars (Amini, Laurencin, & Nukavarapu, 2012). Bone defects are caused by a broad spectrum of events including trauma, infection, old age, chronic diseases, cancer and birth deformities (Rodriguez, Lara-Padilla, & Dean, 2018). Nowadays the only option to treat this is by autologous and cadaveric implants. Autologous implants involve taking bone grafts from some other part of the patient's body, while cadaveric implants take bone tissue from cultivated bones coming from cadaveric bodies. These treatment options could lead to complex issues regarding the patient's health. Nearly 30% of this type of transplants end in infection or other problems (Yeatts & Fisher, 2011). An alternative treatment is the one in study, TE. TE has the potential of addressing current limitation that tissue transplant has, like infection, high cost, insufficient donors, and patient morbidity.

Critical size defects are those that represent a loss that makes it impossible for the body to heal by itself (Kheirallah & Almeshaly, 2016). When it comes to finding an alternative method of treatment, TE alone does not fulfill the requirements, because of the size of the needed piece. But bioreactors along with TE techniques can solve this issue.

#### 2.1.2 Bioreactor for Bone TE

Bioreactors are used to perform many biological reactions under controlled conditions in many areas. Pharmaceutical industries use them to grow yeast or bacterial to produce vaccines or antibiotics. But in TE a bioreactor is used to ensure cell survival of a 3D growing construct helping it mature and proliferate by delivering the essential nutrients in an adequate way and removing toxic waste (Orlando, 2014) . A minimum flow rate of 1 ml/hour has shown to increase cell viability in 3D constructs (Volkmer et al., 2008).

There are different types of bioreactors such as spinner flasks, flow perfusion systems and rotating walls, all of which show great result in dynamic bone tissue engineering allowing nutrients, oxygen, and waste flow as in living organisms (Zhang et al., 2010). A perfusion bioreactor uses a pump mechanism to deliver media through all the scaffolds (Yeatts & Fisher, 2011). This bioreactor can work with direct or indirect flow depending on where the media flows. When the flow goes around the scaffold, it is an indirect perfusion mechanism. If the media flows through the scaffold, it is called a direct perfusion bioreactor. The difference between these two mechanisms can be seen in Figure 2. Direct perfusion bioreactors have shown to ensure a homogeneous flow through all the scaffold (Yeatts & Fisher, 2011), therefore this is the type of bioreactor that was chosen as the fundamental model for this project.

Flow rate has also shown changes in the differentiation process of undifferentiated cells (De Luca et al., 2020; Kleinhans et al., 2015; Saueroova et al., 2019). Mechanical stimuli that the cells perceive because of the flow makes them differentiate easier and increase their expression of osteoblasts markers. Kleinhans et al. has shown that dynamic culture upregulates these genes compared to static culture conditions.

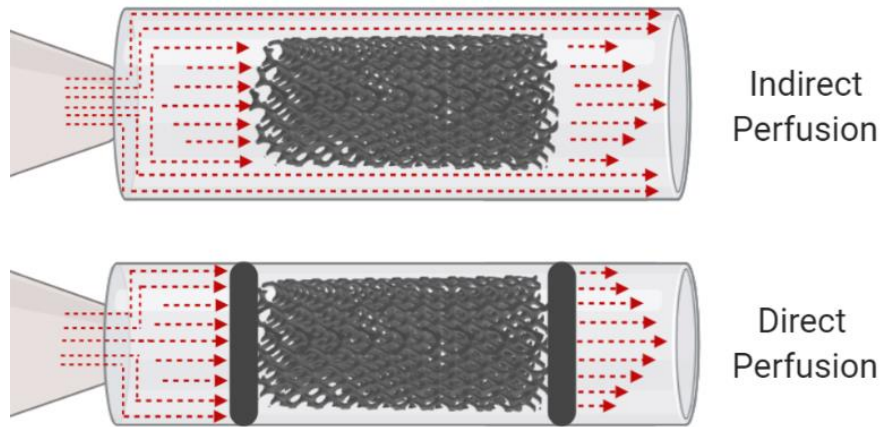


Figure 2. Difference between indirect and direct perfusion

### 2.1.3 Poly- (propylene fumarate) (PPF) as bone TE material

But there is another variable that must be addressed to have a viable and functional tissue sample. Scaffolds and its manufacturing technique must be compatible with the application they will be working with. Scaffolds represent the support the tissue need during its expansion and development. To do so, the scaffold must have specific characteristics that mimic the ECM to compensate the lack of one in *in-vitro* 3D cell culture. One of the most important factors that must be consider during the design of a scaffold is the material used. Biocompatible materials are those that create a desired effect with its surrounding tissue. Its behavior can go from inert to biodegradable in a desire time. Commonly used biocompatible materials are polymers, ceramics, composites of polymers and ceramics and metals (Hutmacher, 2000).

Cells interact directly with the scaffold, meaning that, to create functional tissue, the characteristics of the scaffold must be specific for each application. Porosity, degradation rate, biocompatibility, elasticity, hardness and strength play an important role in the successful development of the desired tissue (Walker, Bodamer, Krebs, et al., 2017). For bone TE, the scaffold used must be able to promote bone tissue regeneration, have augmented surface area, mechanical strength, 3D interconnected pores and a degradation rate similar to bone regeneration rate (Rasheed et al., 2018).

A material that has shown promise in the field is PPF (for chemical structure see Appx. A). PPF is a biocompatible photocrosslinkable polyester designed for bone TE (Shanfeng Wang, Lu, & Yaszemski, 2006). Studies have revealed that PPF has a proper cell adhesion and is not toxic (Mishra et al., 2016). Another characteristic that makes PPF suitable for bone TE is that its degradant composites (fumaric acid and propylene glycol) are eliminated through natural metabolic pathways and its degradation rate emulates the time of bone tissue regeneration.

### 2.1.4 Related Work

Table 1 shows data about the most recent data available regarding bioreactors used for bone TE. Critical factors taken into account were characteristics and manufacture technique, the bioreactors flow type and rate; cell culture parameters, and finally improving tools, such as simulations or sensors.

Reference	Scaffold			Bioreactor		Dynamic Cell culture			Characterization		
	Material	Fabrication process	Scaffold Size (mm)	Type **	Flow Rate (mL/min)	Cell type	Culture Period (days)	Seeding Density (cells / scaffold)	Assays	Simulation	Sensors
(Behrens et al., 2020)	PDMS	Casting	....	L	0.46-1.6	HUVEC	1	...	DAPI-Phalloidin staining	No	No
(Shuang Wang et al., 2020)	PLLA-PLC nanoyarn	Electro-spinning	D= 6 z= .25	P	....	BMSC	14	...	H&E, DAPI, SEM	No	No
(Nokhbatolfoghaha et al., 2020)	$\beta$ -TCP, gTCP (coat)	Foam-casting	7 x 7 x 7	R & P	1.0-2.0	BFPdSC	24	1x10 <sup>6</sup>	qRT-PCR, ALP, SEM, flowcytometry, Glu, IHC, ARS	No	No
(De Luca et al., 2020)	PLLA / nHA	TIPS	1 x1 x .5	P	1.2 (initial), 0.3 (after 6 hrs.)	hMSC	21	5x10 <sup>5</sup>	dsDNA, qRT-PCR, SEM, OsteoImage Mineralization	No	No
(Kim et al., 2019)	ACS sheets & collagen sponge	Purchased	....	IES	....	New Zealand rabbits	7	....	Micro-CT, MTHCS	No	No
(Lovecchio et al., 2019)	Chitosan-graphene	Casting	...	P & C	1.0-5.0	hBMSC	7	1x10 <sup>6</sup>	LIVE/DEAD, von Kossa	FEM	Temp., pH
(Shalumon et al., 2019)	Gelatin / nHAP cryogels	Molding	D= 1	P	....	BMSC	14	4x10 <sup>3</sup>	ALP, SEM/EDS, LIVE/DEAD, Actin/DAPI, ARS, OCN ELISA, qPCR,	No	No
(K. T. Lim, Patel, Seonwoo, Kim, & Chung, 2019)	2D Culture	...	...	IP	0.01-34.0	hBMSC	21	...	WST-1, e CyQUANT, ALP,	CFD	pH, DO, O <sub>2</sub> , CO <sub>2</sub> , temp., press.
(Yaghoobi, Hashemi-	nHA-PCL	Electro-spinning	z= .12	DP	4.5-2.0	hMSC	7 & 14	15x10 <sup>3</sup>	Ca, MTT, ALP, SEM, RunX	No	No

Najafabadi, Soleimani, & Vasheghani-Farahani, 2019)											
(Sauerova et al., 2019)	COL, PDLLA, bCaP, HYA	Lyophilization	D=6	P	0.03	pMSC	7 & 14	2x10 <sup>5</sup>	Dapi, qRT-PCR, eQuant-iTTM	No	No
(Vetsch, Betts, Müller, & Hofmann, 2017)	Silk fibroin	β-sheet formation	D=8 z=3	IP	0.2-12.0	hMSC	40	5x10 <sup>5</sup>	alamarBlue, ALP, eQuant-iTTM, H&E, von Kossa	CFD	No
(Kanda et al., 2016)	Collagen sheets	....	z=3	RF	3	rBMC	7	5x10 <sup>5</sup>	DNA-based cell count, H&E, ALP, IHC	No	DO, pH, temp.
(Kleinhans et al., 2015)	PLLA-co-PCL	Solvent casting & salt leaching	D=10.5 z=25	P	0.8	hMSC	7	5x10 <sup>5</sup>	Ca, qRT-PCR	CFD	Press.

\*\*\* Bioreactor Type: C: compression, DP: direct perfusion, IES: Implantable electrical stimulation, IP: indirect perfusion, L: laminar, P: perfusion, R: rotational, RF: radial flow

Table 1. State of the Art in Bone TE Bioreactors

### 2.1.5 Objective

The majority of *in-vitro* tests are made with 3D culture in scaffolds using static cell culture method with the disadvantage of the formation of necrotic cores, especially in implants larger than usual (distance from its center of about 100-200  $\mu\text{m}$ ). This is mainly caused by the uneven distribution of nutrients and oxygen and the accumulation of toxic cell waste (Volkmer et al., 2008a).

Volkmer et al. made culture constructs with preosteoblasts and conducted a Live/Dead assay to describe the behavior of this type of cells in static culture. Appx. B shows alive cells in green and dead ones in red, after 3(A), 5(B) and 7 (C) days of static culture. It can be seen by the red area that cells start to die from the center out from day 5 and almost cover the entire construct during day 7 (Volkmer et al., 2008a). Uneven oxygen and nutrient perfusion are a conflict of interest regarding 3D cell culture. Its low solubility and deficient diffusion capacity make it difficult to culture large cell constructs using a 3D technique (Volkmer et al., 2008a).

Considering the problematic statement of deficient nutrient and oxygen distribution and waste exchange in large 3D cultures, a perfusion bioreactor was designed and validated to be used for bone TE with PPF scaffolds. This is the approach taken to diminish necrotic core in large cell constructs grown in a 3D environment. Generating a uniform flow that totally perfuses the scaffold will eliminate uneven oxygen and nutrient distribution, as well as toxic cellular waste, diminishing necrotic core and inducing a homogenous proliferation and differentiation in cells growing in a PPF scaffold.

The general objective of this project is to design, develop and validate a perfusion bioreactor that generates a minimum flow rate of 1 ml/hour which can be used to diminish necrotic core during 3D bone TE in PPF scaffolds. The bioreactor must have the following characteristics:

- Affordable and done with commercially available parts
- Modular
- Easy to sterilize with an autoclave
- Biocompatible
- Able to resist being inside an incubator (37°C, 5% of CO<sub>2</sub>)



## 2.2 Materials and Methods

The following section describes the protocols and exercises done during the development process of the bioreactor. The section is divided in design, prototyping and validation. Cell culture techniques, starting from the initial proliferation and ending with cell characterization techniques, are also defined in this segment. The process to do so is described in Figure 3, showing the tasks done during each stage of the project. How this process was done will be described in this section.

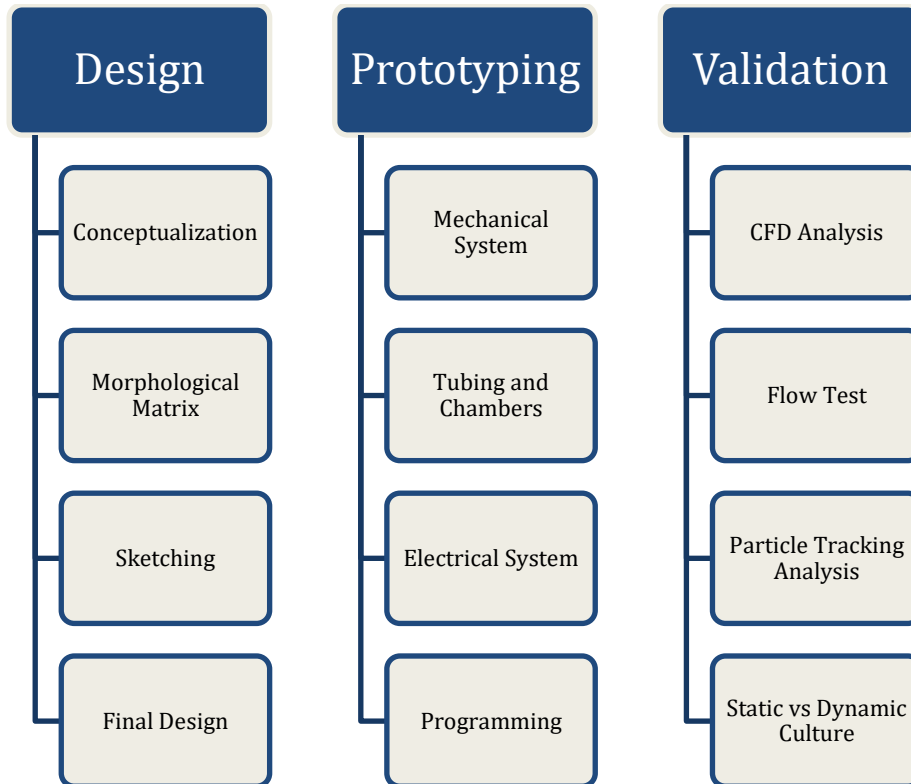


Figure 3. Perfusion Bioreactor Development

### 2.2.1 Design

To start designing the perfusion bioreactor, a clear and concise idea of what it is needed must be established as a solid base, starting with the most important characteristics that need to be fulfilled. As a global specification, all parts must be cheap, commercially available, replaceable and if they have contact with cells or the cell incubator, they have to be autoclavable. The bioreactor needs three basic modules to work, a flow generator, incubation chambers, and a control system.

For the flow generator, precision, and accuracy its needed. The mechanical system has to be reliable and able to give a constant flow for a long period of time, since it will be left working for more than 12 hours without supervision. A system that can be able to recirculate media in a closed loop is desired. Cellular media is replaced every two days to prevent cell waste concentration and provide enough nutrients, but there is no need to use new media for every circulation cycle. And finally, the flow generator must not be in direct contact with media or cells because it may cause contamination.

For the flow to be modulated a control system has to be able to regulate the peristaltic pump. It is desired that this system can be easily manipulated for it to have the ability to change its configuration if it is needed. This could be useful to generate more than one flow velocity and be used for different applications. Also, it must be compatible with different platforms and be able to generate the voltage and amperage needed to move the peristaltic pump.

The incubation chambers refer to the space designated for the scaffold in which the cells will grow. Flow must be able to pass through all the scaffold in the incubation chambers, so the design must meet this important criterion. They need enough space for the scaffold to be taken in and out, but it also must be able to fixate the scaffold to force flow to go through it and not around it. Chambers must endure the pressure that the flow might exert on their inner walls. Sterility is another major requirement for these chambers since avoiding cell contamination is key to have a successful construct.

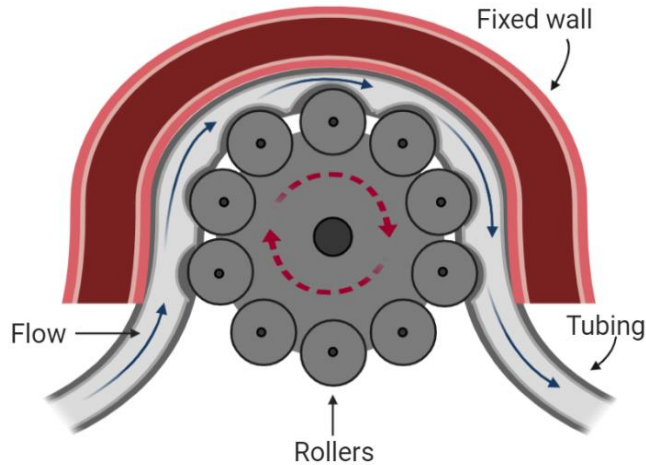
After the specifications of each module were stated, a morphological matrix showing the different options available that meet the criteria was made to combine the possibilities and decide the best approach. This design tool is a visual approach to capture the functional alternatives and combinations, giving a wide range of possible design solutions (Moultrie, n.d.). The purpose of a morphological matrix is to explore all the options available and create design solutions combining the feasible elements in the matrix.

Once the morphological matrix provided possible design solutions, sketches of the solutions were made with the purpose of integrating the elements and figure out which one works the best for the purpose. The combination of the possible designs were linked by colors, that is how each of the solutions can be identified. Sketches were done and can be seen in Appx. C. After deliberating using the sketches, the final design was chosen.

### **2.2.2 Prototyping**

Mechanical system was purchased as well as the motor to move it. Chambers were done using 3 ml plastic syringes cut to have only the cylindrical part of the middle. The same plungers in the syringes were used to seal the chamber and to fix the scaffolds inside the chambers. Electrical system is composed of a power supply, a stepper motor driver and a microcontroller. All system is controlled by a program that consist on controlling the delay time between each 1/8 step.

A DG4 Multi-channel Head ® with ten rollers by Chongqing Jieheng Peristaltic Pump Co., Ltd ® (Chongqing, China) was used as the mechanical system of the pump. Its working mechanism is illustrated in Figure 4. This head has space for four lines and can change the pressure exerted on them. This model has the option of expanding the lines using only one motor by stacking head pumps one in front of the other and coupling them. This provides the opportunity of running multiple lines for large experiments at the same time with only one control system (for reference see Appx. D).

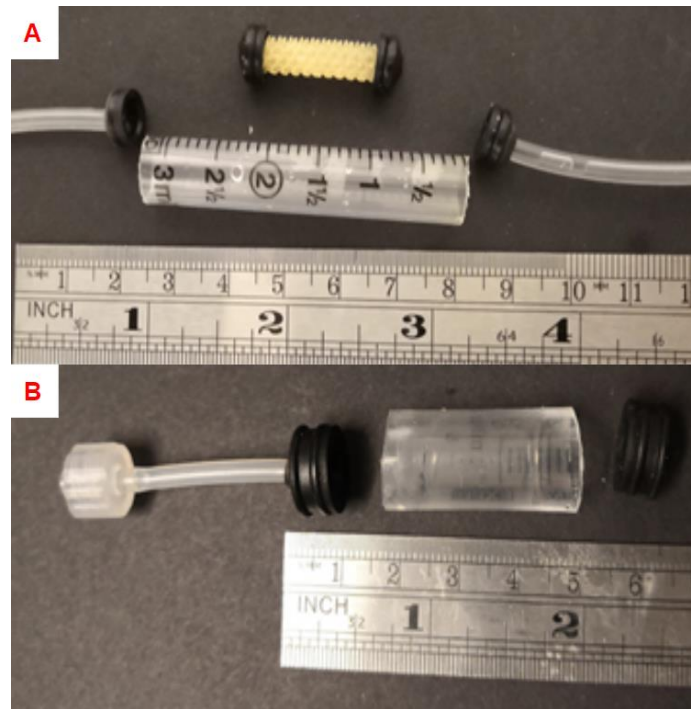


**Figure 4. Working mechanism of the roller peristaltic pump used in the prototype**

As an actuator a Nema 23 was coupled in the back of the head. This is a hybrid bipolar stepper motor with high torque. Using a high-power motor will ensure that the rollers will rotate even when the pressure between the hose and the fixed wall is high. To control it with an Arduino platform a Stepper Motor Driver Board (WINGONEER TB6560 3A Single-Axis Controller, China) was used with an Arduino Uno microcontroller board (HiLetgo, Shenzhen, China). To power the system a 12V-3A power supply is used. All the circuitry including the power supply were placed in a plastic box and a DC ventilator was used to avoid the components to overheat. The electric schematic of the control system is illustrated in Appx. E.

The Arduino code used to run the bioreactor is also found in Appx E. The code is configured to run as slowly as the motor is able, but by changing the `intPause` variable to a lower number the motor will go faster, and the perfusion pump will deliver a greater flow.

Lines consist of tubing, a bubble trap and the chamber that holds the scaffold. 1/8"-diameter permeable tubing (C-Flex, Cole-Parmer, Vernon Hills, IL, USA) was used for the connections between bubble trap, chamber and media reservoir. Chambers and bubble traps are fabricated with 3 ml plastic syringes. Scaffolds are fixed in the chambers with two plunger seals, one on each side of the scaffold. Chambers, scaffold fixation, and a bubble trap are shown in Figure 5.



**Figure 5. Line components separated view A) Chamber with tubes, scaffold, and scaffold fixations. B) Bubble trap.**

The pump, tubing system and media reservoir are intended to go inside the incubator, since these components are in direct interaction with cells. While the control system goes outside the incubator, only connected to the stepper motor by cables going into the incubator through a specially modified plug on the back of the incubator.

### 2.2.3 Validation

To validate the system designed a series of experiments were done to ensure the system delivers what it should and that the flow was able to perfuse through all the scaffold. Cell assays were also performed to validate the efficiency of the system in maintaining alive cell constructs with significant size.

#### 2.2.3.1 *CFD Analysis*

A computational fluid dynamics (CFD) simulation was done to ensure complete scaffold perfusion. Using Flow Simulation in SolidWorks® (Dassault Systèmes, Vélizy-Villacoublay, France) a flow trajectory and a particle tracking analysis were performed. As boundary conditions, inlet flow velocity was inserted in the inner face of the left closing lid and to give it a way-out atmospheric pressure was inserted in the inner face of the right closing lid. Simulation ran with a mesh specificity of 6, gravity activated, and water parameters, with a computational domain that enclosed all the construct. In the particle tracking analysis, particles had a diameter of .001 mm.

#### 2.2.3.2 *Flow Test with Particle Tracking*

A flow test with an open loop of the configuration shown in Figure 11 was performed for 24 hours to quantify the volume the bioreactor was delivering. The line of the bioreactor was made by 1/8"-diameter permeable tubing (C-Flex, Cole-Parmer, Vernon Hills, IL, USA) with an internal diameter of 2 mm and chambers made of 3 ml plastic syringes with an internal diameter of 9.65 mm. After the time period ended, the water was measured with a 1000 µl pipette with a resolution of 1 µl. Using the decomposition of flow,

$Q = Av$ , the average velocity within the chamber and the hoses was found. To validate the flow test data, a microfluidic device with fluorescent microparticles and video analysis were done. A 6 x 6 x 6 mm cubic scaffold with squared 1.5 x 1.5 mm pores like the one shown in Image 6 was printed using an EnvisionTEC Perfactory® 3 (EnvisionTEC, Dearborn, MI, USA) with EnvisionTEC's E-Shell 300 Series resin. The scaffold was then placed in a microfluidic device with a channel of 5 mm. The microfluidic device was made using Polydimethylsiloxane (PDMS) with a molding technique utilizing an aluminum mold as the one shown in Figure 6E and sealed with glass slide using an oxygen plasma reactor after the scaffold was inserted. The bioreactor was connected to the microfluidic device by puncturing the devices chambers with a 3 mm biopsy puncher to insert the tubing. Yellow-green 1.0  $\mu\text{m}$  Invitrogen FluoSpheres™ ( Thermo Fisher Scientific, F13081) were diluted in PBS at a concentration of  $6 \times 10^7$  spheres/ml (Stoodley, DeBeer, & Lewandowski, 1994) and injected into the lines with a syringe. Once the FluoSpheres™ solution was flowing through all the system, the bioreactor was left running a couple of minutes to stabilize the flow. The microfluidic device was introduced to a Nikon A1R HD25 confocal microscope, as shown in Figure 6F, and positioned the lenses at 700 $\mu\text{m}$  from the bottom with a 10X magnification in the center of the scaffold. 2-minute videos were taken using denoise function and around 1.33 s per frame. The frame taken was in the center pore of the scaffold with a complete pore in sight, as shown in Appx. G. Using a velocity probe in uScope software, particle velocity was measured. The pore was divided in 9 sections (as seen in Figure 13) and measures were taken in all of them. Around 230 sample points were taken to average them and get the average velocities in each section. Velocity vectors in a perfusion pump like the one used in this bioreactor do not have a constant direction, it changes between rollers causing a backwards flow ( $Q_b$ ). Appx G shows the vectors of particle velocity while going forward and backward. Forward flow ( $Q_f$ ) and  $Q_B$  averages were then used to determine the distance the particle traveled while going forward and backwards. Next the distances were subtracted and this way the total distance of the particle per cycle was obtained using Equation 1 and 2.

$$(vQ_f \times 8) - (vQ_b \times 3) = d_{\text{cycle}}$$

**Equation 1. Distance in each cycle considering the displacement in  $Q_f$  and  $Q_b$**

$$\frac{60}{11} \times d_{\text{cycle}} = Qv_{\text{average}}$$

**Equation 2. Total average flow rate velocity in a minute**

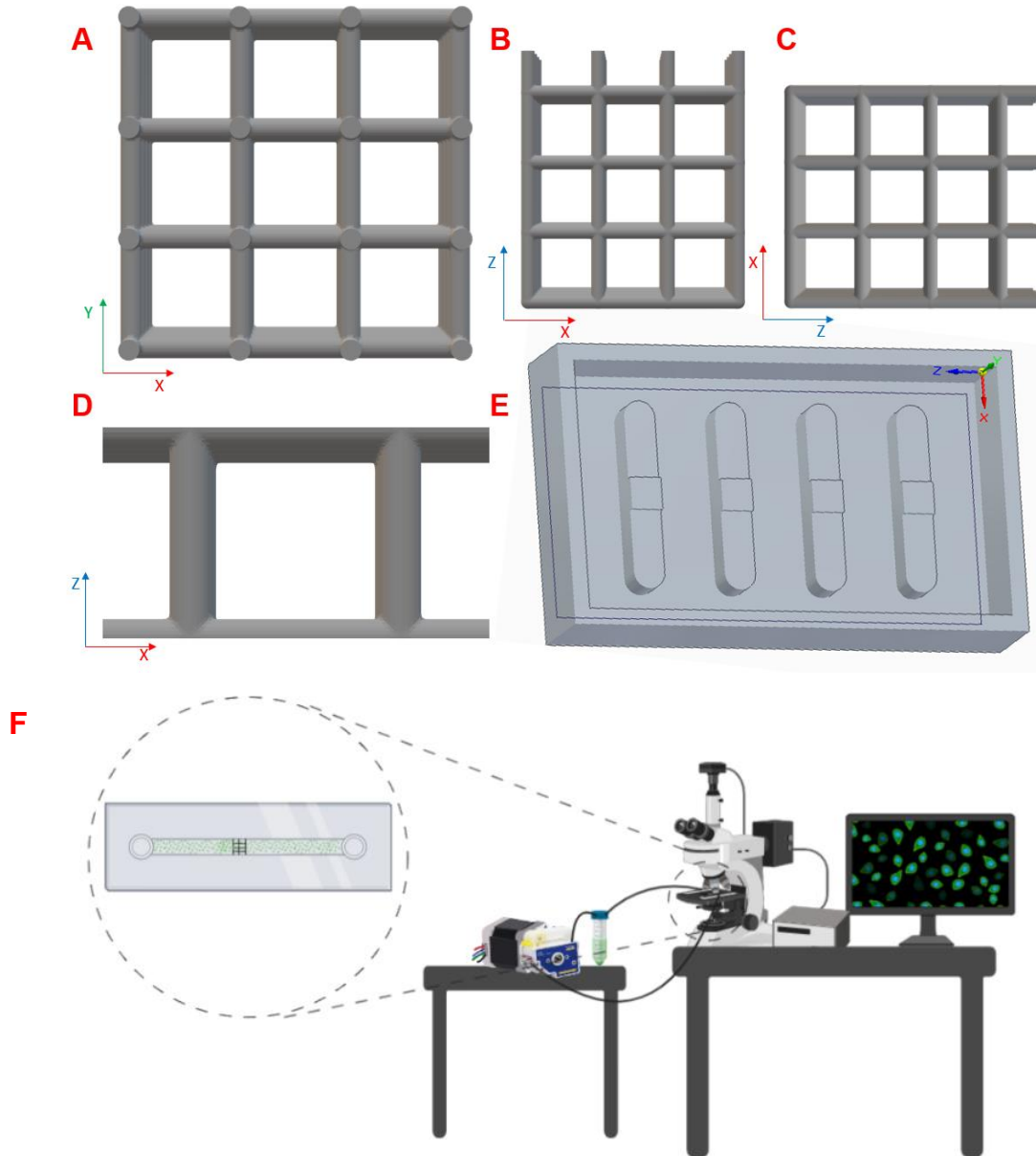


Figure 6. CAD design of the scaffold used for particle tracking and mold A) Upper view B) and C) Lateral view D) Strut details E) Aluminum mold used for microfluidics device F) Microscope, bioreactor and microfluidic device layout

### 2.2.3.3 Static vs Dynamic Culture

Static and dynamic culture experimentation groups were done. The experimental plan is illustrated in Figure 6.

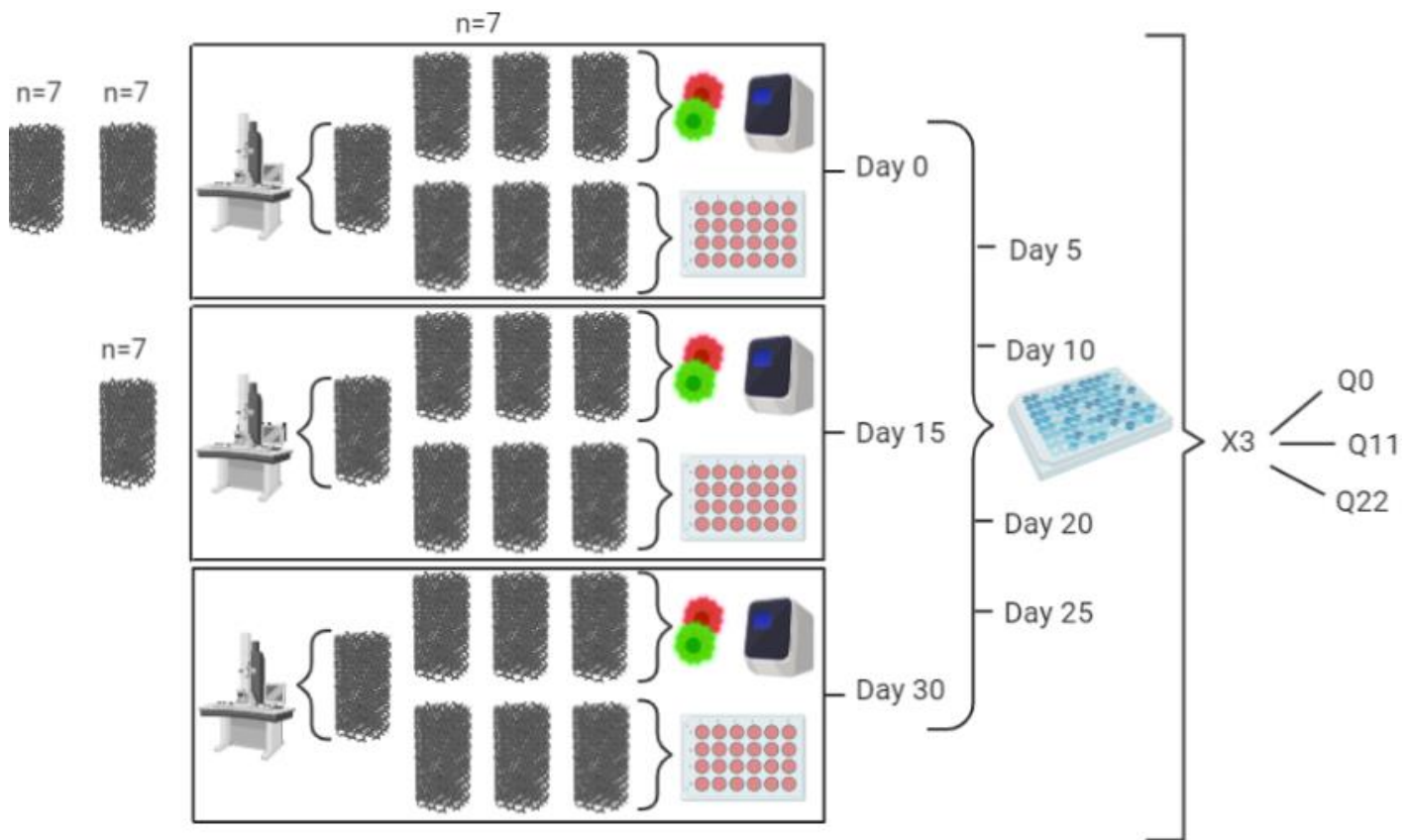


Figure 7. Static and dynamic characterization plan

**PPF Resin Preparation** Pure PPF resin is viscous and does not have the rheological properties to be used in a 3D printer. To use it a 1:1 ratio solution was made with diethyl fumarate (DEF, Sigma–Aldrich, St. Louis, MO) and 1400 Da PPF resin previously synthesized by ring opening method (Luo et al., 2016). Irgacure 784 and bisacylphosphine oxide (BAPO) (Ciba Specialty Chemicals [BASF], Tarrytown, NY) were used as photo initiators with a .4% and 3% concentration, respectively. As a final ingredient acting as a light attenuator, 2-hydroxy-4-methoxybenzophenone (HMB; Sigma Aldrich, St. Louis, MO) was used.

**PPF Scaffold fabrication** PPF cylindrical scaffolds with a diameter of 6 mm and height of 25 mm were manufactured using a 3D DLP printer as shown in Appx F. .STL files of the scaffolds with an internal Schoen gyroid geometry and pore architecture consisting of 200  $\mu\text{m}$  struts and 700  $\mu\text{m}$  pores, resulting in a designed porosity of 88.2%, as the one shown in Figure 8; were generated using MATLAB code. After turning on the printer and letting it warm for 15 min, the calibrating process was done to ensure the mask light intensity was the same in all the platform. A 48-field mask adjustment was made to set light intensity compensation mask to 180  $\text{mW}/\text{dm}^2$ . Using the resin formulation described earlier, scaffolds were 3D printed using an EnvisionTEC Perfactory® 3 (EnvisionTEC, Dearborn, MI, USA) with a layer thickness of 50  $\mu\text{m}$ , irradiance of 350  $\text{mW}/\text{dm}^2$ , and projection time of 30 s. After the printing process, uncured resin was washed away with acetone and graded ethanol. To sterilize them for cell culture, a solution of 49% acetone, 21% ethanol and 30% distilled water is made to put the scaffolds in the sonicator for 25 min. They were



later removed and submerged in sterile PBS for 5 min. This was done thrice and then left in sterile PBS to autoclave them in the liquid cycle.

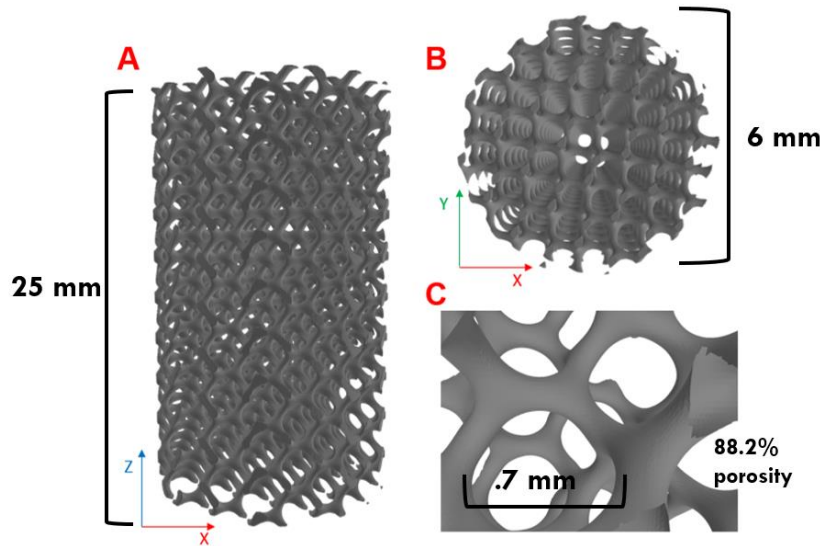


Figure 8. CAD of scaffold used for cell culture A) Lateral view B) Front view C) Schoen gyroid strut details

**Expansion** Xeno-Free Human Bone Marrow-Derived Mesenchymal Stem Cells (hMSCs) were purchased (RoosterBio Inc., Frederick, MD, USA) at passage #2 and expanded to proliferate enough cells to culture them later under static and dynamic conditions. To do so, cells were seeded in T175 culture flask (Corning Inc., Concord, NC, USA) and incubated at 37°C and 5% CO<sub>2</sub> for 7 days. Minimum essential media (MEM) supplemented with 10% FBS and 1% penicillin-streptomycin antibiotics was used and changed every 2 days. Cells were subcultured once to get the desired number of cells.

**3D Culture** After being trypsinized and counted using a hemocytometer and Trypan Blue staining to differentiate dead cells from alive, cells were seeded at a seeding density of  $2 \times 10^6$  cells per scaffold. PPF scaffolds were previously soaked in FBS for 24 hrs. to promote cell adhesion by integrating albumin to its surface. Seeded scaffolds were incubated in standard cell culture conditions in an ultralow attachment six-well plate for 3 days to promote cell adhesion and expansion in the scaffolds. MEM supplemented with 10% FBS and 1% penicillin-streptomycin antibiotics was used and changed every 2 days. Seeded scaffolds were then moved into the bioreactor chambers and fixed with plunger seals, as shown in Figure 5, inside the biosafety cabinet. Everything was previously sterilized with an autoclave in the instrument cycle. Scaffolds were then divided in three groups, two of them were connected to a bioreactor, one was cultured for 30 days under a flow rate of 11 ml/hr., while the other one was cultured under other group under a 22 ml/hr. flow rate. The last group was left in the chambers without any flow for 30 days. Osteogenic media (MEM with 10 mM Na-β-glycerophosphate and  $10^{-8}$  M dexamethasone and 0.2 mM of ascorbic acid) was used during this part of the experiment and changed every 2 days.

**PrestoBlue® Assay** A metabolic assay can monitor cell proliferation and let cells live normally afterwards, as it is not a destructive assay. This provides the opportunity to know how cells are managing between the time point established for other destructive assays. PrestoBlue® Cell Viability Reagent (PB) (Thermo Fisher Scientific, A13261), solution must be handled in the dark since it is a light sensitive solution. Scaffolds must be carefully transported to a six well plate on days 0, 5, 10, 15, 20, 25, 30. A 1:10 solution of PB in cell culture media was made. After aspirating the remaining media of the scaffolds, PB solution was pipetted in the well until the scaffold was completely covered in solution. The same amount is pipetted into all the well plates and left in the incubator for an hour. One hour later 100 μl of each sample was pipetted in triplicate into a clear bottom 96-well plate. Samples were returned to the bioreactor chambers after being



cleaned carefully with PBS and refilled with clean media. The solution in the clear bottom 96-well plate was then read in multiwell plate reader (Molecular Devices, CA) configured for fluorescence with excitation wavelength of 560 nm and emission wavelength of 590 nm. Data was normalized with control samples and graphed to be compared

**Calcium Mineralization Assay** To determine mineralization cause by osteogenic differentiation, cross section samples representing the 3 regions of the scaffold (as Figure 9A shows) from day 0, 15 and 30 were washed twice with PBS and fixed with 4% paraformaldehyde for 15 min at 4°C. .5% Alizaren Red solution is prepared in PBS resulting in a solution with pH 4.2. After fixation, cells were covered with the staining solution prepared earlier and left 10 min at room temperature. Once time passed samples were washed five time with PBS and observed under a brightfield microscope. Images were then taken to Image J to quantify the mineralized area. After subtracting the background image, total color contrast was measured, and the mineralized area was calculated.

**LIVE/DEAD Assay** To quantify cell viability, scaffolds where taken in days 0, 15 and 30 and cut with a scaffold to get a center view of the of scaffold as shown in Figure 9B. Samples where then washed with PBS, rinsed, and incubated for 15 min in clean PBS. Calcein AM (0.5  $\mu\text{L}/\text{mL}$ ) and ethidium homodimer-1 (2  $\mu\text{L}/\text{mL}$ ) were mixed and diluted in PBS. Samples were taken out of the incubator, rinsed, and covered completely with the stain solution. After 1 hour of incubation, samples where drained and washed twice with PBS. Samples were then seen under a fluorescent microscope (Zeiss Axiovert 135). Once starting to work with the stain everything was done under low light conditions. Cell viability was determined using Image J (National Institute of Health, USA) to see the total of living and deceased cells and calculating the ratio of the living and total cells.

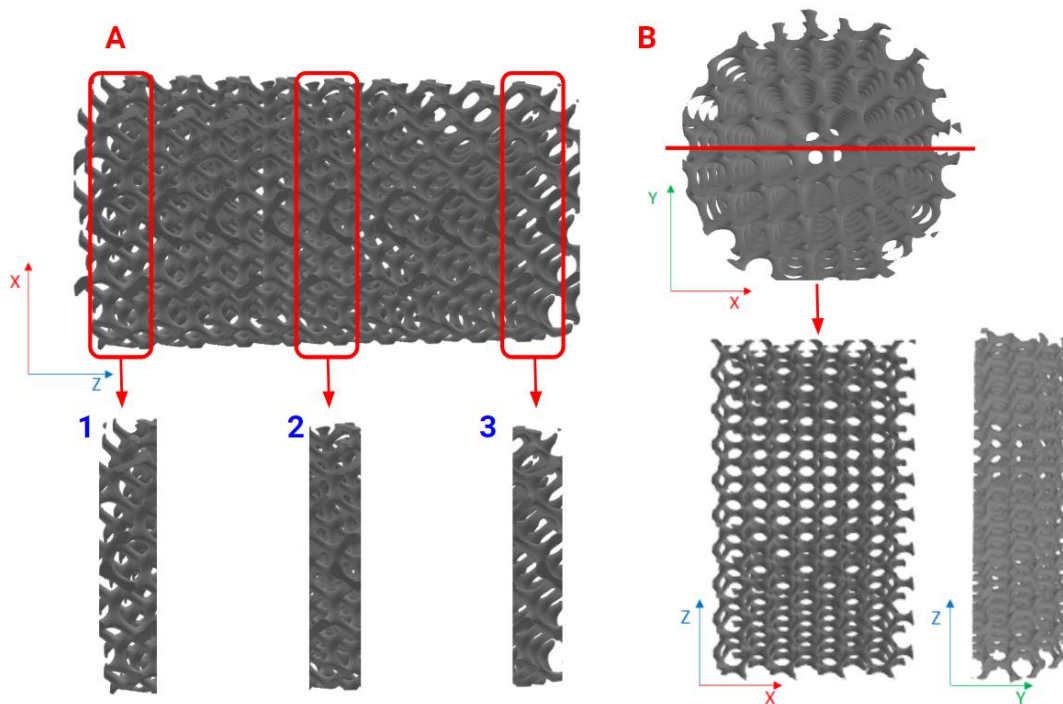


Figure 9. Cross section of significant regions in the PPF scaffold. A) Lateral view showing section 1, 2 and 3 used for Calcium Mineralization Assay B) Frontal cut on x axis used in Live/Dean Assay

**SEM Imaging** Three samples from each group for each time point were prepared for SEM imaging as follow. After washing the samples with PBS three times, they were fixed with 4% paraformaldehyde for 15 min at 4°C. For image contrast enhancement, samples were treated with OsO<sub>4</sub> for 30 min and then dehydrated in graded ethanol (from 50% to 100%) and dried. Sample must be conductive to be seen under a scanning electron microscope, since the sample in matter does not have conductive properties it had to be gold plasma coated using a sputter coater. Using 5kV, a spot size of 3 and a working distance range o 6-7 mm, SEM images of the samples were taken.

**RT-qPCR** To extract RNA from the samples, PureLink™ RNA Mini Kit (Invitrogen, 12183020) was used according to the manufacturers protocols and recommendations (Appendix C). To synthesize cDNA, 1 µg of RNA was used with SuperScript III First-Strand Synthesis SuperMix (Invitrogen, Inc.). Using a 20ul reaction mixture with 1ul of template containing 500 nmol/L of gene specific primers and 1nm/L of Bio-Rad SYBR Green Master Mix (Bio-Rad Laboratories, Inc.) of GAPDH, ALPL, BGLAP, BMP-2, COL1A1, RUNX2 PCR primers, RT-qPCR analysis was done. Conditions for Denaturalization to occur were 95°C for 1 min 45 cycles of 95 °C (15 s), 56 °C (15 s), and 72 °C (15 s); and a final extension at 72 °C for 5 min.

**Statistical Analysis** Experimental and control groups were analyzed in triplicates (n=3). A technical triplicate was also done in all the measurements collected. To compare experimental and control groups data, a one-way ANOVA was used and to verify the statistical difference with 95% confidence (p<0.05), a Tukey's multiple comparison test.

## 2.3 Results

Design, prototyping, and validation results are shown in this section. Cell characterization experimentation was planned but not done, so the expected results are described both, written and with figures as visual aids.

2.3.1 Design

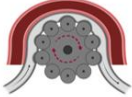


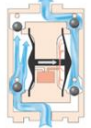

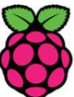





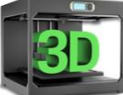
	Option 1	Option 2	Option 3	Option 4	Option 5	Possible Combinations
Flow Generator (F)	 Roller peristaltic	 Syringe	 Rotary pistons	 Rolling diaphragm	 Linear peristaltic	<ol style="list-style-type: none"> <li>1. F1+C1+I3</li> <li>2. F2+C3+I1</li> <li>3. F1+C2+I2</li> <li>4. F5+F3+I4</li> </ol>
Control System (C)	 RaspberryPi	 ARDUINO				
Incubation Chambers (I)	 Glass syringe	 Plastic syringe	 Six-well plate	 3D printing		

Figure 10. Morphological matrix for bioreactor design with possible combination

The morphological matrix shown in Figure 10 provides five options for pumps that could be used in the design, three data acquisition platforms for the control system and four options for the base of the incubation chambers. Although the options that are presented on the matrix can provide dozens of options, last column of Figure 10 presents four possible designs incorporating the more adequate elements for the working principals of this project.

From the options generated by the matrix sketches were done. Appx C contains the sketches that were helpful to visualize, generate discussion about design issues and finally decide what proposal to develop according to the needs of the project. After deliberating the advantages and disadvantages of the proposed designs, it was decided that the proposal that provides the greatest fidelity to what is sought in the project was combination number 3.

2.3.2 Prototyping

A graphic representation of the complete system is shown in Figure 11.

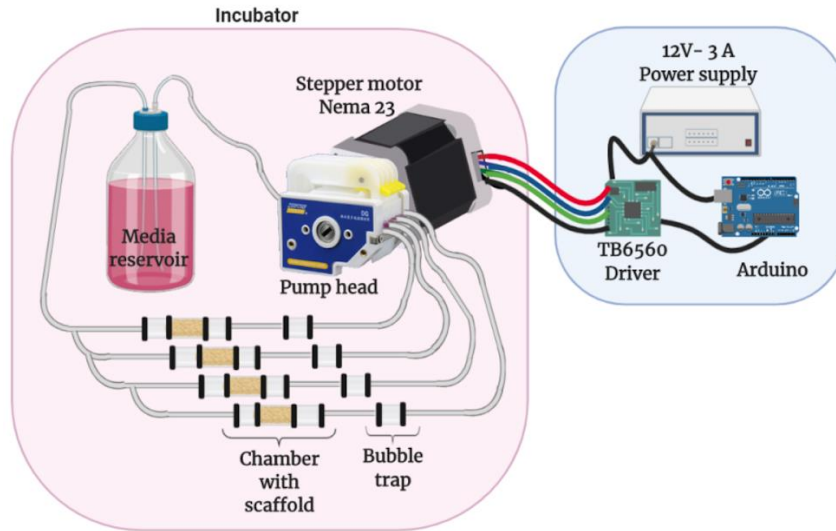


Figure 11. Bioreactor final prototype

### 2.3.3 Validation

#### 2.3.3.1 CFD Analysis

Flow trajectory analysis demonstrated that, with the flow velocity delivered by the bioreactor ( $5.22 \times 10^{-4}$  m/s) and the configuration in which the scaffold is fixated, media reaches all the scaffold, being able to transport nutrients and oxygen even to the center of the construct. Figure 12A shows the results of the flow trajectory analysis and Appx G contains a video of the animation of the flow. As seen in Figure 12B, the particle tracking analysis has similar results, as particles travel along all the scaffold.

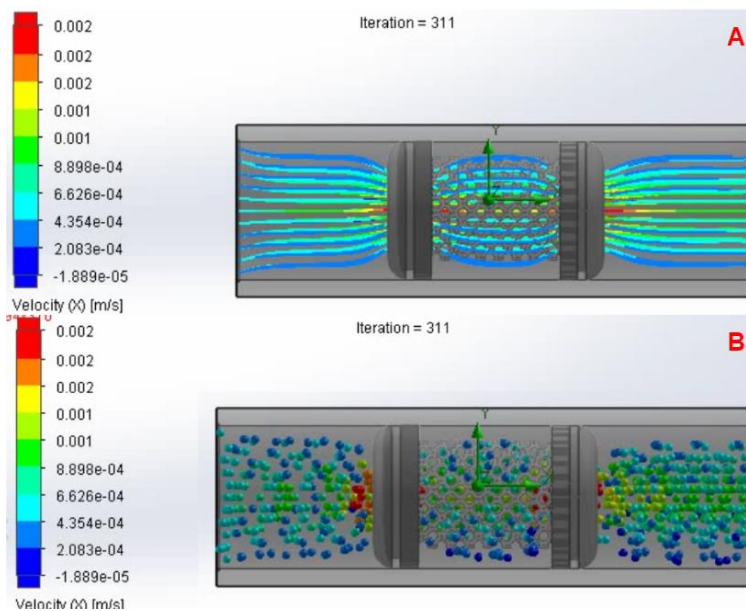


Figure 12. CFD results. A) Flow trajectory. B) Particle tracking.

Table 2 shows shear stress and relative pressure that were also calculated in this simulation as well as min, max velocities in x, y, and z axis. Shear pressure present in the construct is similar to the one present in the body (0.05 -12 Pa) (Uygun, Uygun, & Yarmush, 2011), meaning it does not cause damage to the cells.

Name	Minimum	Maximum
Velocity (X) [m/s]	-1.889e-05	0.002
Velocity (Y) [m/s]	-3.583e-04	3.652e-04
Velocity (Z) [m/s]	-3.396e-04	3.830e-04
Vorticity [1/s]	6.65e-05	1.78
Relative Pressure [Pa]	-32.85	45.15
Shear Stress [Pa]	1.27e-07	0.02

Table 2. CFD simulation results

### 2.3.3.2 Flow Test with Particle Tracking

The average flow delivered during manual calibration was 11 ml/hr while the average velocity was found to be  $5.07 \times 10^{-4}$  m/s.

The printed square scaffold used during this test was characterized to test the fidelity of the printing process. As seen in Figure 13, the scaffold is 6 x 6 x 6 mm with 1.5 mm pores. Different views, details and the scaffold in the microfluidics device chamber can be seen in Figure 13.

Particle tracking analysis showed the normal behavior of a perfusion pump, in which the flow goes forward and backwards because of the roller holding and releasing the hose. The particular cycle of this mechanism lasts 11 seconds, of which 8 seconds represent  $Q_f$  and 3 seconds  $Q_b$ . With the data analysis of the velocities taken from the microfluidic device in the 9 regions of the scaffold's pore, the average velocity of the particles was  $5.22 \times 10^{-4}$  m/s. Appx. G has the Excell spreadsheet with the calculations done. Figure 14 shows the velocity profile in all 9 sections of the pore as well as the velocity probe used to make the calculations.



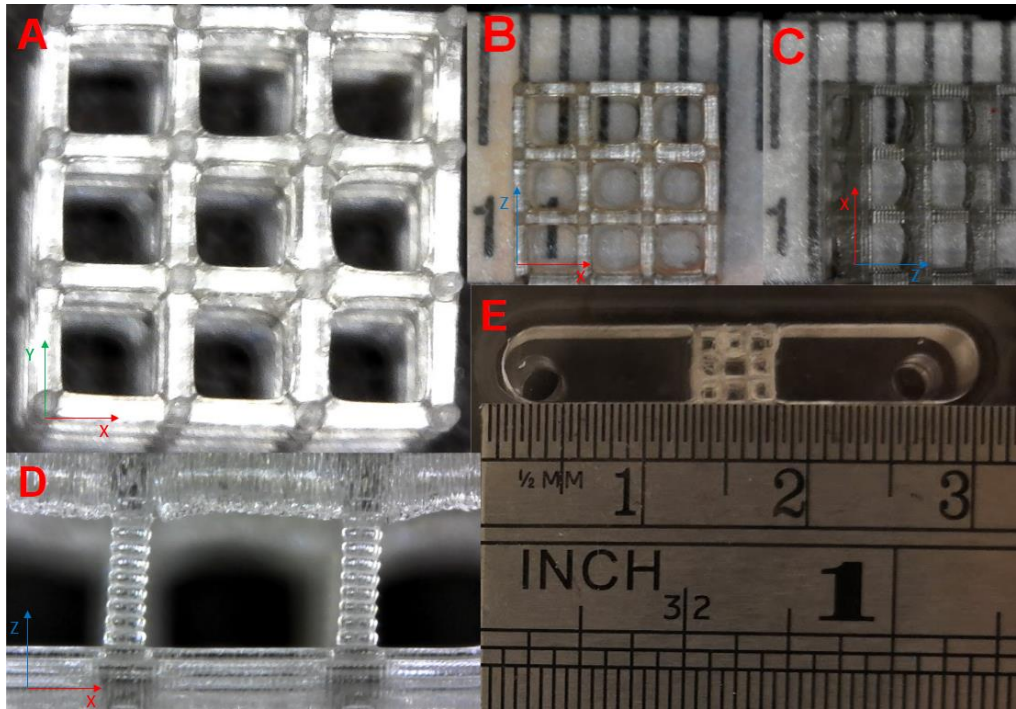


Figure 13. Scaffold used for particle tracking A) 3X magnification B) Upper view C) Lateral view D) 5X magnification showing strut details E) Scaffold in the microfluidic channel

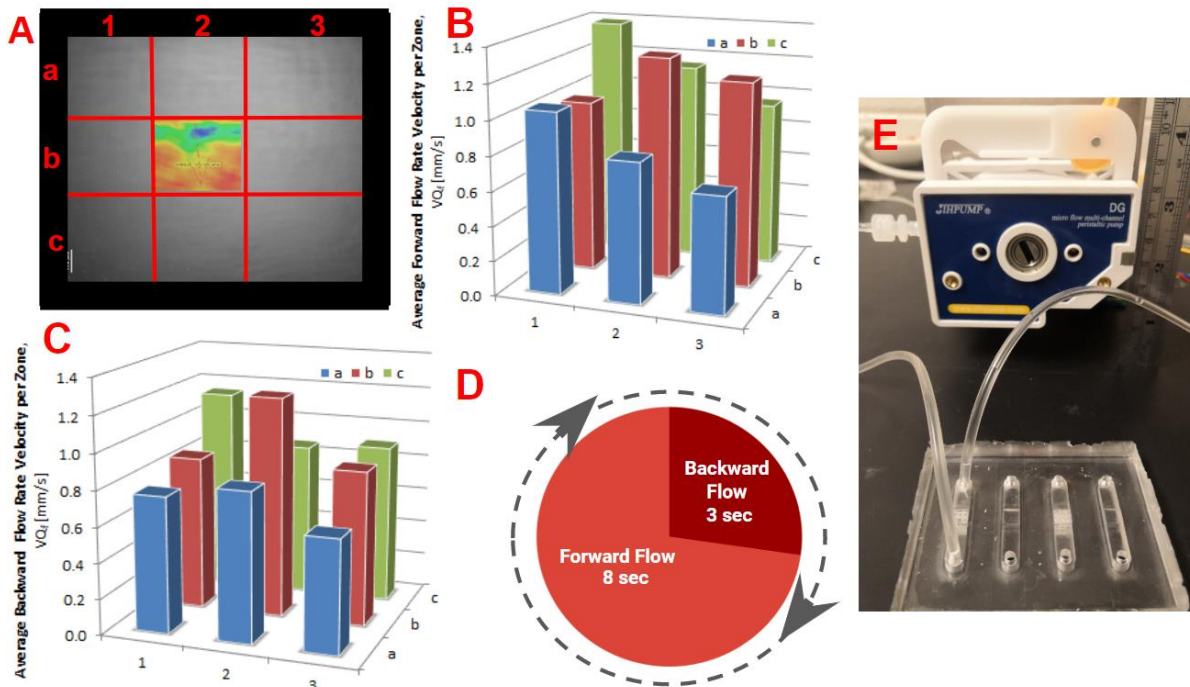


Figure 14. A) Screen shot of the tracking particle video showing a velocity probe in b2 region as representation of the division made to obtain data of all the pore, the scale bar represents 100 $\mu$ m B) Average forward flow rate velocity per zone graphic on which each bar represents a region of the pore using the same distribution as in Figure 14A C) Average backward flow rate velocity per zone graphic D) A pie diagram representing the 11

seconds perfusion cycle in which 8 sec. the flow goes forward and 3 sec. it goes backwards E) Bioreactor and microfluidic device connected

	Average Forward Flow Rate Velocity, $VQ_F$ [mm/s]				Average Backward Flow Rate Velocity, $VQ_B$ [mm/s]		
	a	b	c		a	b	c
1	1.04322	0.80585	0.66521	1	0.76229	0.83378	0.63027
2	0.99595	1.28589	1.17912	2	0.86091	1.23455	0.86622
3	1.38637	1.14685	0.95268	3	1.14211	0.86163	0.89496

**Table 3. Average Forward and Backward Flow Rate Velocity per zone**

**PrestoBlue® Assay** Q0 represents the sample that was left in static culture, Q11 the sample cultured under a 11 ml/hr. flow rate and Q22 is the sample cultured under 22 ml/hr. flow rate. Cell viability is expected to have different results in the study groups. Day 0 represents the beginning of dynamic culture, so Q0, Q11 and Q22 results are very similar. While time passes cells start to grow and cover all those scaffolds under dynamic culture, while cells in static culture start to decrease. By day 15 cell metabolism in Q11 and Q22, represented by fluorescence, stabilizes, and stays the same during until day 30, with an exception in Q11 that decreases a low percentage of its metabolic activity. On the other hand, Q0 decreases in every time point. The complete behavior can be observed in Figure 15.

**LIVE/DEAD Assay** A representation of the expected microscopy images taken from a frontal cut on x axis or the complete scaffold (Figure 9B) of the three types of samples. After the staining procedure in day 0, 10 and 15 are shown in Figure 16. During day 0 cell distribution is very similar, since it is the starting point, but since all groups were under static culture, it can be appreciated that we present some red spots representing cells starting to die. After 15 days of dynamic culture, Q11 and Q22 have a lot more cell density than Q0. A cluster of dead cells is visible in the middle of the Q0, since the construct has more than 200  $\mu\text{m}$  in diameter, the lack of oxygen and nutrients diffusion starts to kill cells in the center. Even though Q11 shows better results than Q0 in this time point, there is still a small portion of the construct that presents necrosis, as shown in Figure 14. By day 30 a significant difference can be seen between static and dynamic culture. More than 60% of the cells in the Q0 are dead while Q11 and Q22 present an even distribution along all its surface. As seen earlier, Q11 has more cell death than Q22, but it is still viable tissue.

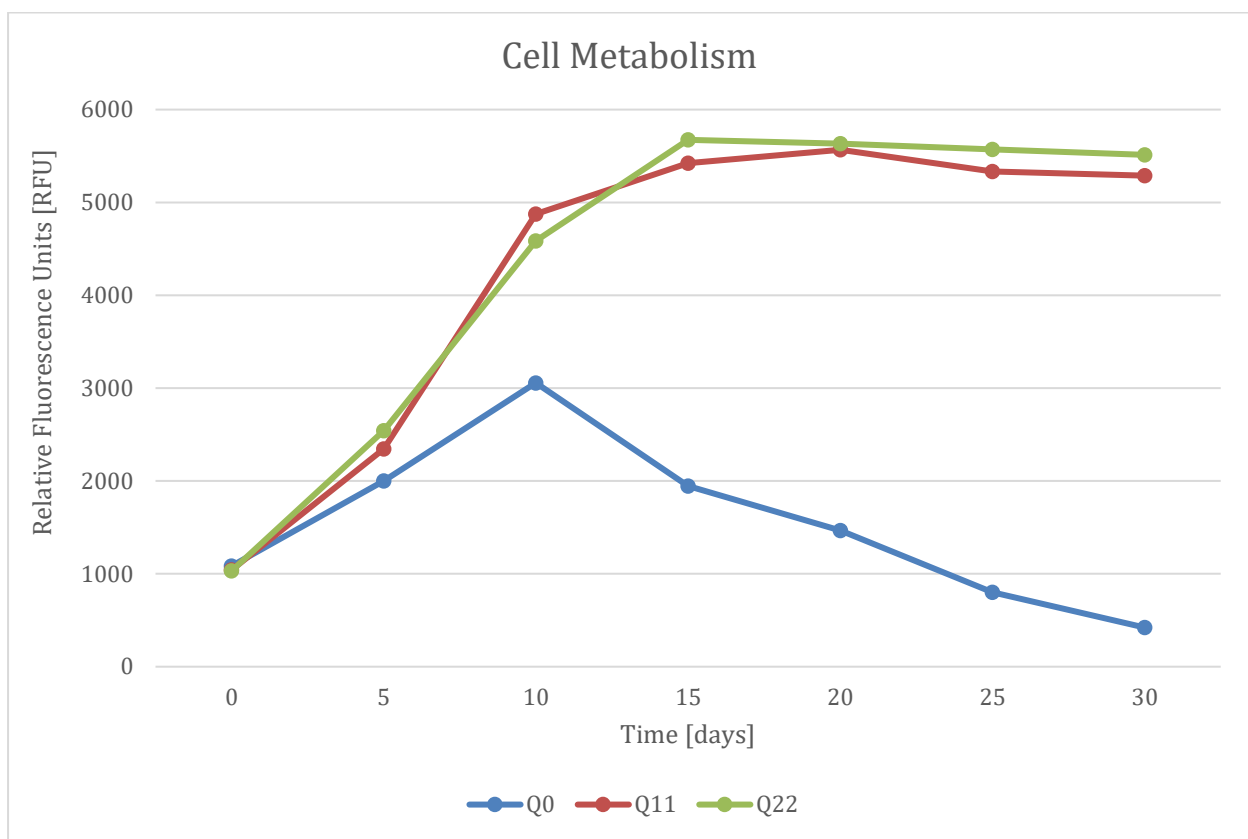


Figure 15. Fluorescence in RFU representing cell metabolism in Q0, Q11 and Q22



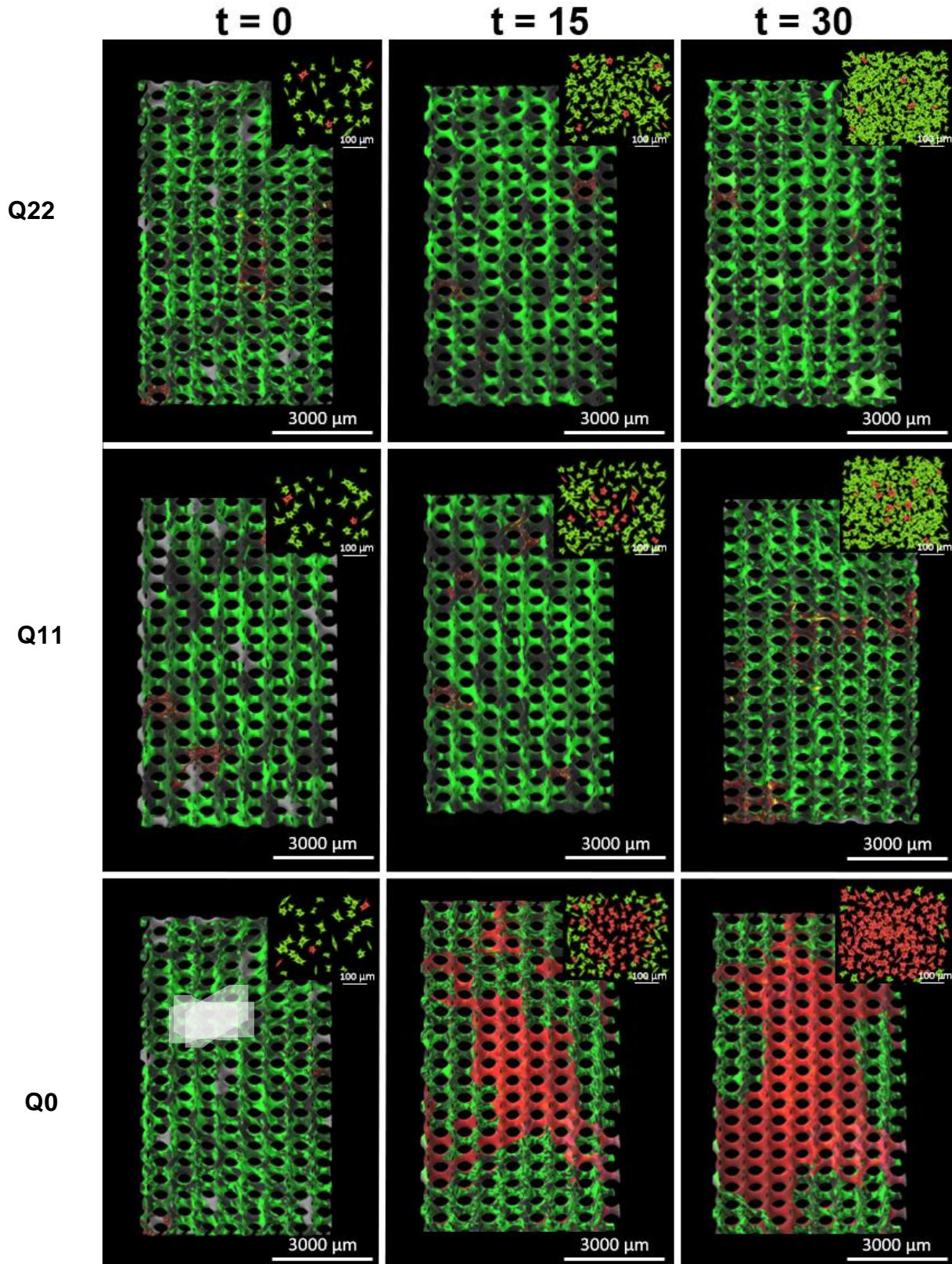


Figure 16. LIVE/DEAD microscopy showing a 1.5X and a 250X representative image of the three study groups at the three time points.

*Calcium Mineralization Assay* ALS staining expected results are shown in Figure 17. Mineralization is proportional to the dye intensity in the scaffold. Q11 and Q22 in day 30 show mineralization throughout all the scaffold, stating that apart from being confluent as seen with the viability assay, cells are differentiating towards osteoclasts during dynamic culture. Since osteogenic media is given to all treatments, Q0 also presents some mineralization, but not much compared to scaffolds under dynamic culture. During day 30 Q0 shows minimum mineralization in the same amount as in day 0 or day 15, stating that mineralization happened at the beginning and stayed in the scaffold for the rest of the experimental period.

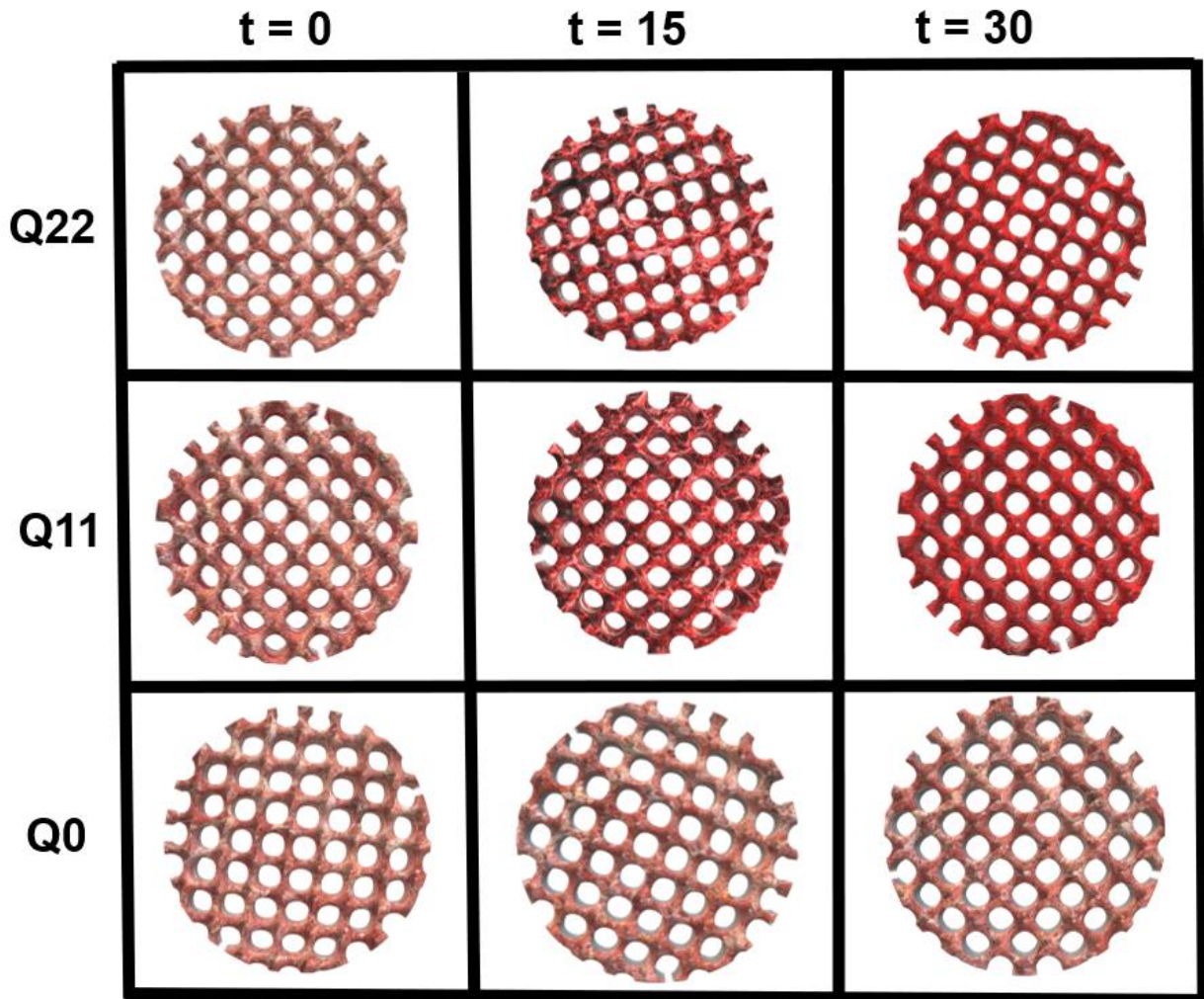
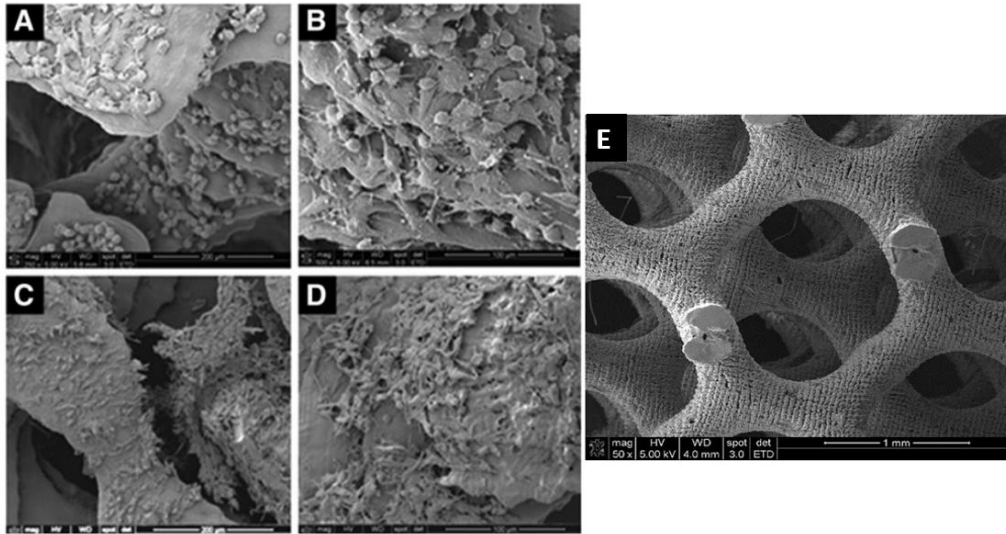


Figure 17. SBC and SSC after ARS in days 5, 10 and 15



**SEM Imaging** A control image was taken before cells were seeded in the scaffold to compare it to when cells grow in it (Figure 18E). As time passes, it can be observed that calcium mineralization is deposited in the surface of the scaffold changing its original morphology.



**Figure 18. SEM images of the seeded scaffolds, A) Cells showing a round morphology at seeding day 2500xB) 3000x C) Spread cells after 7 days of culture 2500x D)3000X (Mishra et al., 2016) E) Scaffold details without cells (Walker, Bodamer, Kleinfehn, et al., 2017)**

**RT-qPCR** using GAPDH as a housekeeping gene ALPL, BGLAP, BMP-2, COL1A1, RUNX2 should be expressed more in Q11 and Q22 than in Q0 and increase while time does. Between Q11 and Q22 there should be a difference too but since, differentiation depends on a lot of factors it is difficult to speculate which one will have an increased expression.

## 2.4 Conclusions and Future Work

A viable and working direct perfusion bioreactor was developed using affordable and commercially available pieces. It is also modular, easily sterilized, biocompatible and able to support incubator environment. Flow given by it is enough to cause a significant improvement in cell survival and differentiation than cell growing under static culture. CFD analysis demonstrated that flow passes throughout all the scaffold including the core and that the shear stress cause by the flow is harmful for the cells. In accordance with the tracking particle analysis demonstrating that all particles with a .001mm diameter of smaller can go through all the pores in the scaffold. This means smaller particles like O<sub>2</sub>, Glucose and other nutrients will not have problems reaching the center of the scaffold. The results that will be obtained confirm that dynamic culture under low flow conditions obtained by a perfusion bioreactor promote cellular survival and development in PPF scaffolds, this is a major step to obtain cultured bone tissue of relevant size to be implanted substituting analogues and cadaveric implants. Future work related to this project involves gene expression, optimizing flow for bone TE and working with other scaffold size and geometries.

### **3 Tumor-in-a-Chip / Cancer Models**

#### **3.1 Introduction**

Cancer is the second leading cause of death in the world, only after cardiovascular diseases, responsible for 1 in 6 deaths globally. According to the World Health Organization (WHO), in 2018, 9.6 million people died due to cancer related issues. This is why cancer industry has an economic impact of more than US\$ 1.15 trillion annually. Among the types of cancer, breast cancer represents the second most common type, with around 2.09 million new cases each year, being one of the five cancers with most common causes of cancer death (WHO, 2018). Finding its pathological physiology is key to combat this disease and is a priority concern for researchers and doctors all over the world.

As technology develops and new techniques emerge, producing new and more reliable models of study has been possible. This can help ease the time and monetary problem that represents finding new treatments, since less than 10% of developed drug make it through clinical trials due to poor predictors of clinical efficiency (Rodrigues et al., 2018). It is also important to notice that cancer has a unique behavior in each patient, it does not always act the same. This makes it more difficult to treat, since not all patients react the same to commonly administrated drugs. For a correct treatment personalized medicine plays an important role, providing doctors with the opportunity to prescribe the correct drug doze and combination (Bashraheel, Domling, & Goda, 2020).

The complexity of this disease caused by unrestrained cell growth, evasion of antigrowth factors and apoptosis, its ability to spread to other parts of the body and staying alive by inducing angiogenesis makes it difficult to replicate in vitro (Weiswald, Bellet, & Dangles-Marie, 2015). Tumor microenvironment plays an important role and must be considered when studying cancer physiopathology. Cancer models nowadays are trying to avoid using 2D culture, organoids and animal models because they are deficient in fidelity, stability and complexity of human physiology (Trujillo-de Santiago et al., 2019). It is important to incorporate the 3D architecture of the tumor that involves cell to cell signaling, ECM support, physical interactions, and different gene expression profile (Friedrich, Seidel, Ebner, & Kunz-Schughart, 2009; Nashimoto et al., 2020; Paek et al., 2019; Pradhan et al., 2018; Shirure et al., 2018; Sobrino et al., 2016). Spheroids, scaffolds, and microfluidic devices are the most common resources used in the matter, and even when some models incorporate vasculature in their models, they lack size relevance.

Solid tumors tend to develop a necrotic core when they are growing, due to the absence of oxygen and nutrients caused by diffusion problems that start around 200  $\mu\text{m}$  of tissue deep (Agarwal et al., 2017). This is where cell-cell signaling come in handy, cells in the necrotic core start producing vascular endothelial growth factor-A (VEGF-A) as well as other inducers, signaling the need of angiogenesis to survive and keep growing (Hanahan & Weinberg, 2011; Heylman, Sobrino, Shirure, Hughes, & George, 2014). Creating relevant size models is important to replicate this phenomenon in where several growth factors, cell types and proteins are involved. Tumor-on-chip models incorporates microfluidics, tissue engineering and bio-fabrication technique to create a reliable and cost-effective way to recreate a tumor's microenvironment. There are several factors that make this platform a better fit to model human solid tumors because it incorporates 3D nature, structural and dynamic complexity and a better way to characterized and observe (Trujillo-de Santiago et al., 2019). Organ-on-chip devices provide the opportunity to mimic real human tissue under controlled conditions and maintain it a substantial amount of time, giving it reliability during drug tests.

3.1.1 4. Related Work

3D cancer models nowadays use different techniques to help improve the reliability and complexity of the model. Here exhibit is a table comparing recent work in the field incorporating said technique variability.

Reference	Culture platform		Cell culture							Characterization	
	System	Material	Perfusion	Culture in	Chamber/ scaffold size (mm)*	Spheroids	Diameter Size (µm)	Cell type	Culture time (days)	Assays	Drug treatment
(Nashimoto et al., 2020)	Microfluidic	PDMS	External Vascularization	U-bottom well and MF chamber	1	Yes	1159	RFP-HUVECs, hLFs, MCF-7, SW620, MDA-MB-231, HepG2	17	Fluorescence time-lapse imaging and confocal microscopy, H&E, IHC	Paclitaxel
(Paek et al., 2019)	Microfluidic	PDMS	External Vascularization	ECM Hydrogel	1 x 3	Yes	155	NHLFs, HUVECs, hASCs, hAMECs, ACBRI 181, iPSC, HOFC	10	Flow tracers, ELISA, LIVE/DEAD, IHC, SEM, AFM	Paclitaxel
(Meng et al., 2019)	Microfluidic	Silicon	External Vascularization	GelMa hydrogel matrices	3 x 8	No	.....	GFP- M4A4, RFP- HUVECs, A549	12	Panoramic and Time-lapse fluorescence, qPCR	EGF4KDEL, CD22KDEL
(W. Lim & Park, 2018)	Microfluidic	PDMS	Pressurized Media tanks	Concave µwells	0.4	Yes	120	HCT116, U87	3	Live/Dead	Irinotecan

(Pradhan et al., 2018)	Microfluidic	PDMS	Vascularization and syringe pump	PEG-fibrinogen Hydrogel	5 x 5	No	.....	MCF7,MDA-MB-231, BJ-5ta, hBTECs	28	Fluorescent TRITC-dextran perfusion, CellScale Microsquisher, Live/Dead	Doxorubicin hydrochloride, paclitaxel
(Mannino, Pradhan, Roy, & Lam, 2018)	Microfluidic	PDMS	Endothelialized channel	Gelatin/HA hydrogel	4	No	.....	A20, MLMVECs	.....	Micrography, IHC	Anti-CSF-1R
(Michna et al., 2018)	Microfluidic	PDMS	Central vascular channel by a Syringe pump	Collagen Hydrogel	3	No	.....	MDA-MB-231, TIME	3	Live/Dead, SEM, Actic/Dapi, Permeability	No
(Chen, Gao, Wang, Lin, & Jiang, 2018)	Microfluidic and Hydrogels	PDMS	External Vascularization in hydrogels	U-shaped $\mu$ chambers	.2 x .3	Yes	100	HUVECs, HLF, THP-1	6	Immunofluorescent staining, CAM, zebrafish assay	Carbon dots
(Agarwal et al., 2017)	Microfluidic	PDMS	Hydrostatic pressure	Alginate microcapsules and collagen ECM	.8 x .8	Yes	387 $\pm$ 15	MCF-7, HUEVCs, hADSCs	14	qRT-PCR, stress tests, SEM, Live/dead, fluorescence images, In vivo tumorigenesis, H&E, VEGF ELISA	DOX, ICG
(Sobrino et al., 2016)	Microfluidic	PDMS	External Vascularization	Chamber	1.6 x .8	No	.....	ECFC-Ecs, NHLFs, SW620, SW480, HCT116, MDA-MB-231, MCF-7, MNT-1	7	FLIM, SPOT Imaging, mCherry, GFP, Azurite Blue, AngioTool, FITC-dextran perfusion, Immunofluorescent staining, XTT-cell viability assay,	Fluoruracil, Vincristine, Sorafenib, Taxol, Oxaliplatin, Pazopanib, Linifanib, Apatinib, CP-673451, Vemurafenib, Vandetanib, Cabozantinib, Sorafenib

(Singh, Mukundan, Jaramillo, Oesterreich, & Sant, 2016)	Microwell array	PEGDMA	.....	Microwell array	.150, .300, .450, .600	Yes	600	MCF7	6	Ru-dpp, qRT-PCR, immunostaining, size reversal experiment, siRNA transfection	4-Hydroxytamoxifen
(Santoro, Lamhamedi-Cherradi, Menegaz, Ludwig, & Mikos, 2015)	Electrospun scaffolds	PCL	Bioreactor	3D Scaffold	3 x 1	No	.....	ES	10	Quant-iT PicoGreen dsDNA, immunoblot, Flow Cytometry, SEM, DAPI	Doxorubicin hydrochloride
(Kwak, Ozcelikkale, Shin, Park, & Han, 2014)	Microfluidic	PDMS	Pressurized media tanks	Interacting monolayers	1 x 2.7	No	.....	MCF-7, HMEC-1	3	E-cadherin, type IV collagen immunofluorescence	NP transport

### 3.1.2 Objective

Design, fabricate and create a breast tumor-on-chip model with clinically relevant size and long-life span that, in future experiments, facilitates the incorporation of vasculature due to VEGF expression. serve as a relevant in-vitro preclinical model for drug testing.

200-300  $\mu\text{m}$  spheroid will be seeded in the chamber of a microfluidic chip for them to grow and merge. The system incorporates a central channel for media to travel, this will provide nutrients to the core of the tissue construct, supplying the tissue with oxygen and nutrients, avoiding necrotic core. This will facilitate spheroids to grow and incorporate with each other to create a solid tumor the size of the chamber. Figure 18 provides an illustration of the expected evolution of the spheroids thru time.

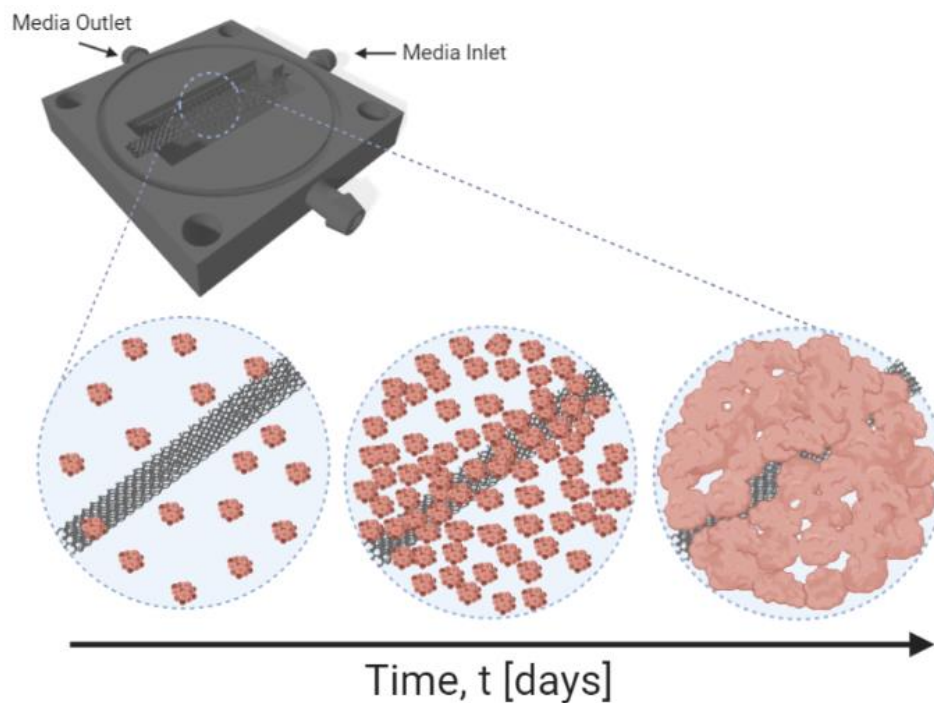


Figure 19. Spheroids dynamic and evolution through its time in the microfluidic chip

## 3.2 Materials and Methods

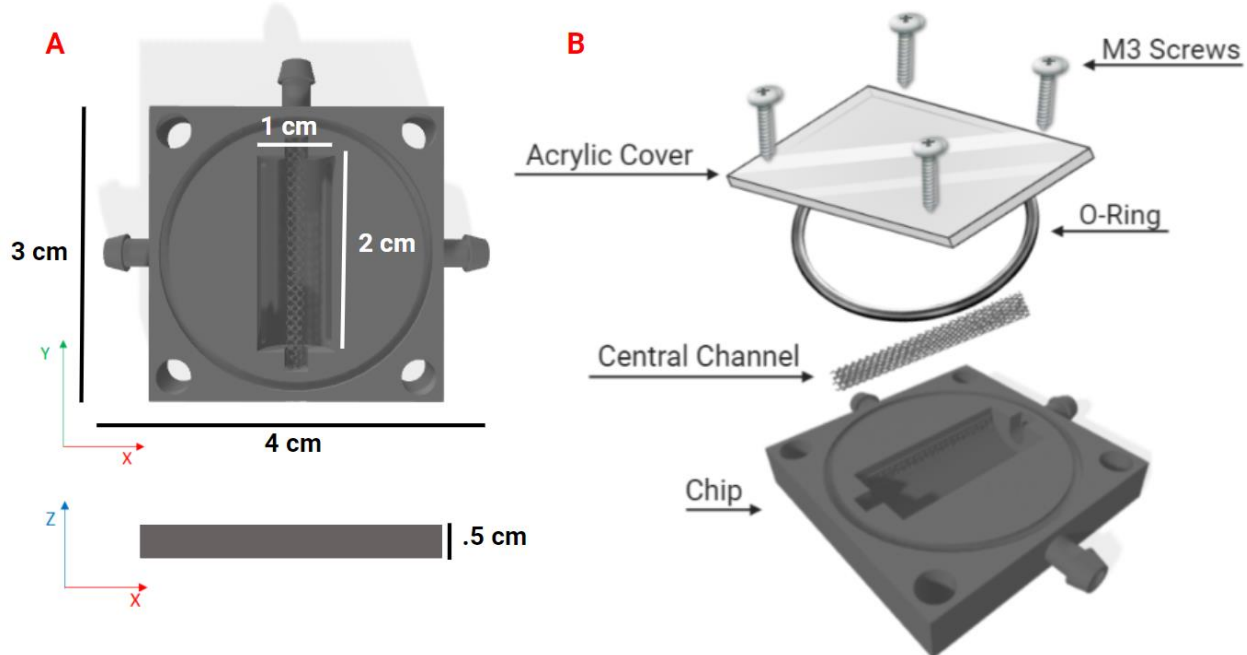
Making use of complex fabrication and cell culture techniques, authors were able to design a chip that supports a tissue construct elevation one step in magnitude order in volume and in lifetime.

### 3.2.1 Chip design and manufacture process

**Design** The chip was designed using SolidWorks® (Dassault Systèmes, Vélizy-Villacoublay, France). The central chamber is thought of as a culture chamber where the central channel is the way media enters the device. Figure 19A shows the device's dimensions in x, y, and z axis. The central channel has a 1.5 mm diameter and Schoen gyroid internal geometry generated with MATLAB code. This geometry facilitates its printing process since it does not need extra support pieces to have a successful printing process. Since the dimensions of the chip are difficult to produce with most manufacturing techniques, design details like not using support to print them are important. A removable channel provides an easy way to visualize and characterize the growing tissue. The acrylic cover also provides a window to monitor the progress of the



system. Figure 19B provides an exploded view of the complete system. The central channel is positioned in the lateral hollow cavities of the chamber, then the O-ring goes in the designed space in the outer part of the chamber, followed by the acrylic cover used to seal the device, with four M3 screws to secure the acrylic cover.



**Figure 20. Chip design A) Dimensions in all directions B) Exploded view of the entire system**

**Manufacture process** The resulted chip design was manufactured using a 3D DLP printer as shown in Appx. F. .STL files were generated from the CAD file made in SolidWorks® (Dassault Systèmes, Vélizy-Villacoublay, France). After turning on the printer and letting it warm for 15 min, the calibrating process was done to ensure the mask light intensity was the same in all the platform. A 48-field mask adjustment was made to set light intensity to 180 mW/dm<sup>2</sup>. Using EShell 300 (EnvisionTEC, Dearborn, MI, USA) resin, CAD models were then 3D printed using an EnvisionTEC Perfactory® 3 (EnvisionTEC, Dearborn, MI, USA) using manufacturer parameters. After the printing process, uncured resin was washed away with acetone and graded ethanol.

### 3.2.2 Tumor-on-chip characterization

This section represents an experimental plan, it is subject to changes or modifications once the testing period begins.

**Spheroids** MCF7 Spheroids were made with a standard protocol under normal conditions and donated by Alvarez-Trujillo Lab in Centro de Biotecnología-FEMSA at Tecnológico de Monterrey campus Monterrey.

**Cell culture in Chip** With a volume of 800 mm<sup>3</sup>, the chip expects around 50% cell growth. 25,000 spheroids in EMEM (10%FBS, 1%PenStrep) were seeded in the chamber and left 2 hours in the incubator under normal cell culture conditions before starting the flow. A constant flow of 16 µl/hr. was maintained for 60 days, with media changes every 2 days.

**Glucose concentration in medium** Glucose concentration from media inlet and outlet was measured with a glucose meter every 4 hrs. the first 3 days. After day 3 it was measured every 12 hrs.

**Cell Metabolism Assay** The first 3 days of chip culture a metabolic assay was done every 4 hours, then every 12 hours. PrestoBlue® Cell Viability Reagent (PB, Thermo Fisher Scientific, A13261) was used. The solution must be handled in the dark since it is a light sensitive solution. A 1:10 solution of PB in cell culture media was made. After aspirating the remaining media of the chips, 500 µl of PB solution was pipetted in the chip and left in the incubator for an hour. One hour later 100µl of each sample was pipetted in triplicate into a clear bottom 96-well plate. Samples were returned to the incubator after being cleaned carefully with PBS and refilled with clean media. The solution in the clear bottom 96-well plate was then read in multiwell plate reader (Molecular Devices, CA) configured for fluorescence with excitation wavelength of 560 nm and emission wavelength of 590 nm. Data was normalized with control samples and graphed to be compared.

**LIVE/DEAD Assay** To quantify cell viability, the central channel and tissue were taken in every 7 days. Samples were washed with PBS, rinsed, and incubated for 15 min in clean PBS. Calcein AM (0.5 µL/mL) and ethidium homodimer-1 (2 µL/mL) were mixed and diluted in PBS. Samples were taken out of the incubator, rinsed, and covered completely with the stain solution. After 1 hour of incubation, samples were drained and washed twice with PBS. Samples were then seen under a fluorescent microscope (Zeiss Axiovert 135). Once starting to work with the stain everything was done under low light conditions. Cell viability was determined using Image J (National Institute of Health, USA) to see the total of living and deceased cells and calculating the ratio of the living and total cells.

**H&E and Immunohistochemical Staining** Every 7 days tumor tissue was retrieved and fixed with a 4% paraformaldehyde (PFA)/PBS dilution to later be sectioned for histological and immunohistochemical analysis. After dehydration and paraffin embedding, samples were H&E stained using standard protocol. Primary antibodies for E-cad, Ki-67, HIF1a and ER were then incorporated as well as its secondary detection system. Images were taken to ImageJ to quantify antigen presence by binarizing positive areas.

**Immunofluorescence Staining** Constructs were taken out of the chip as well as the central channel every 7 days and fixed in 4% PFA for 20 min at room temperature, washed and permeabilized with .5% X-100 for another 20 min. Samples were then treated with blocking solution of 1% BSA for 60 min and incubated with primary antibodies for E-cad, HIF1a, VEGF and Ki-67 diluted 1/100 at 4°C overnight. After washing three times with PBS, samples were left in the dark with Alexa Fluor 633 secondary antibodies 2hrs. at room temperature. Finally, nuclei were stained with DAPI for 10 min and seen on a confocal microscope (LSM 880, Zeiss Carl). Tissue was reconstructed using z-stack with 5 µm slices. 2D images were taken to ImageJ to quantify fluorescence between time points.

**RT-qPCR** To extract RNA from the samples, PureLink™ RNA Mini Kit (Invitrogen, 12183020) was used according to the manufacturer's protocols and recommendations. To synthesize cDNA, 1 µg of RNA was used with SuperScript III First-Strand Synthesis SuperMix (Invitrogen, Inc.). Using a 20ul reaction mixture with 1ul of template containing 500 nmol/L of gene specific primers and 1nm/L of Bio-Rad SYBR Green Master Mix (Bio-Rad Laboratories, Inc.) of GAPDH, E-cad, HIF1a, VEGF, ER and Ki-67 PCR primers, RT-qPCR analysis was done. Conditions for Denaturalization to occur were 95°C for 1 min 45 cycles of 95 °C (15 s), 56 °C (15 s), and 72 °C (15 s); and a final extension at 72 °C for 5 min.

**Statistical Analysis** Experimental and control groups were analyzed in triplicates (n=3). A technical triplicate was also done in all the measurements collected. To compare experimental and control groups data, a one-way ANOVA was used and to verify the statistical difference with 95% confidence ( $p < 0.05$ ), a Tukey's multiple comparison test.

### 3.3 Results

Tumor-on-chip section represent expected results and are only speculations.

#### 3.3.1 Chip design and manufacture process

*Manufacture process* After a couple of tries, the model came from the printer as expected. The central channel needed to be positioned in the center of the printing platform for it to be printed correctly. This can be because the light masks of the printer needed maintenance and were not performing with the detail needed. This could be seen during the mask calibration process in were the outer parts of the masks were not reaching the light intensity need. But as soon as the channels were positioned to be printed in the center of the platform, no problems were encounter. Figure 20 shows photographs of the printed results.

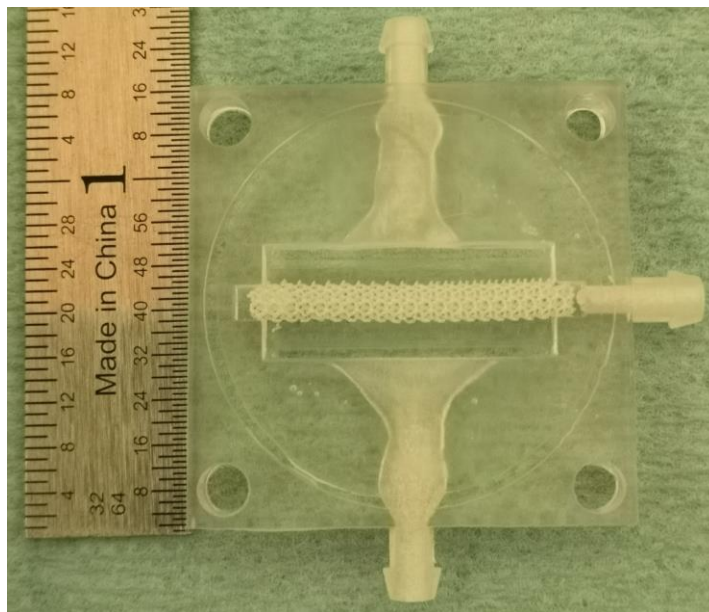
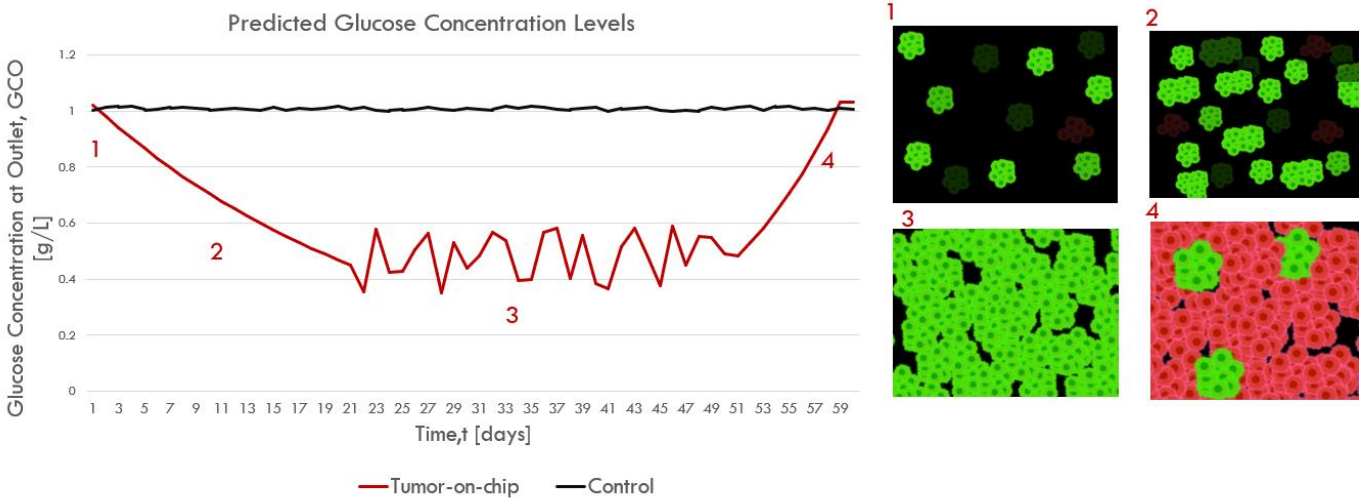


Figure 21. Printed chip with mounted scaffold

#### 3.3.2 Tumor-on-chip characterization

*Glucose concentration in medium* Glucose concentration (GC) at the inlet is 1.02g/L, which is the concentration media has. As time passes GC at outlet decreases due to the cells taking it to survive, grow and expand. It is expected that as cells grow, GC go lower and lower until reaching a steady state. When cells reach confluence in the chamber, GC at the outlet would stay steady thought the days because cells are no longer growing but surviving. This state is expected to last at least until half of the second month of experimentation, this would assure that cells reached their maximum growth capacity and are having a longest live spam due to the nutrients reaching all the construction. As times goes past the second part of the second month, cells would start to die and GC at outlet will start to increase due to the absence of glucose consumption dead cells represented. Figure 21 shows the expected GC at outlet as explained earlier.



**Figure 22. Predicted glucose concentration levels at outlet along 60 days of experimentation and Live/Dead representation during specific time points**

**Cell Metabolism Assay** Results from PrestoBlue Assay will show an opposite behavior than the glucose concentration assay, representing the same cell growth phenomenon. Cells will start to grow considerably, increasing their metabolism, reaching their maximum growth capacity around day 20, maintaining it until around day 50 and losing cells in the last third of the experimental time.

**LIVE/DEAD Assay** An increase of green fluorescence is expected during the first days during cell development. Similar images are expected during the second third of the experimental run, confirming the behavior seen with the metabolic and glucose concentration assays. More red fluorescence, meaning dead cells, will be seen towards the last 10 days of the experimentation period.

**H&E and Immunohistochemical Staining** As time passes the visibility of E-cad on the created tissue will increase. This is since E-CAD is a marker for cell adhesion and as they grow and form bigger agglomerations cell adhesion will increment. Ki-6 and ER are identity markers, these are expected to be uniform along all the experiment, confirming that cells have not mutated or lost some of their functions. Finally, HIF1a is a hypoxia marker, an increase in the tissue volume is expected and even though perfusion is considerably better than in other models, there will be parts that will suffer from lack of oxygen, making HIF1a present.

**Immunofluorescence Staining** Similar behavior as in H&E and Immunohistochemical Staining is expected for E-cad, HIF1a, and Ki-67. VEGF was incorporated to this assay to evaluate its presence and to confirm the need cells express to create vasculature. As time passes, an increase in VEGF is expected too.

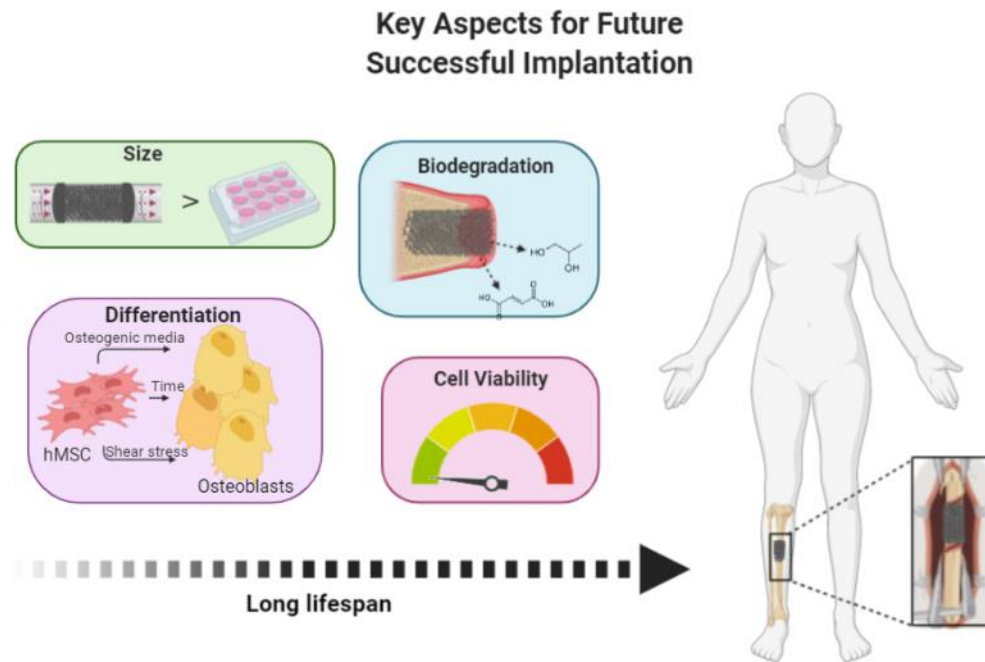
**RT-qPCR** Using GAPDH as a house keeping gene, E-cad, HIF1a, VEGF, ER and Ki-67 expression should be similar to both immunostaining techniques described above, confirming the same behavior.

### **3.4 Conclusions and Future Work**

As a result, the chip designed and created showed a great performance in the manufacture techniques chosen as in the cell culture and tumor creation process. The printed chip is liable to the CAD model in size and geometry. The central channel had no problems printing without any support even with its complex geometry. The DLP printer was tested at its limits and after a few tries, the final result was as good as expected. Solid tumor formation is expected to form around day 7-10 and became visible without a microscope due to the agglomeration and spheroid growth. As future work, the experimental designs must be done and perfected. Once this first round of data is compiled, a second run needs to be done co-culturing endothelial cells to form vascularization and bring complexity and reliability to the model. Drug testing can also be done in the future to test the platforms human modeling fidelity.

## 4 Conclusions

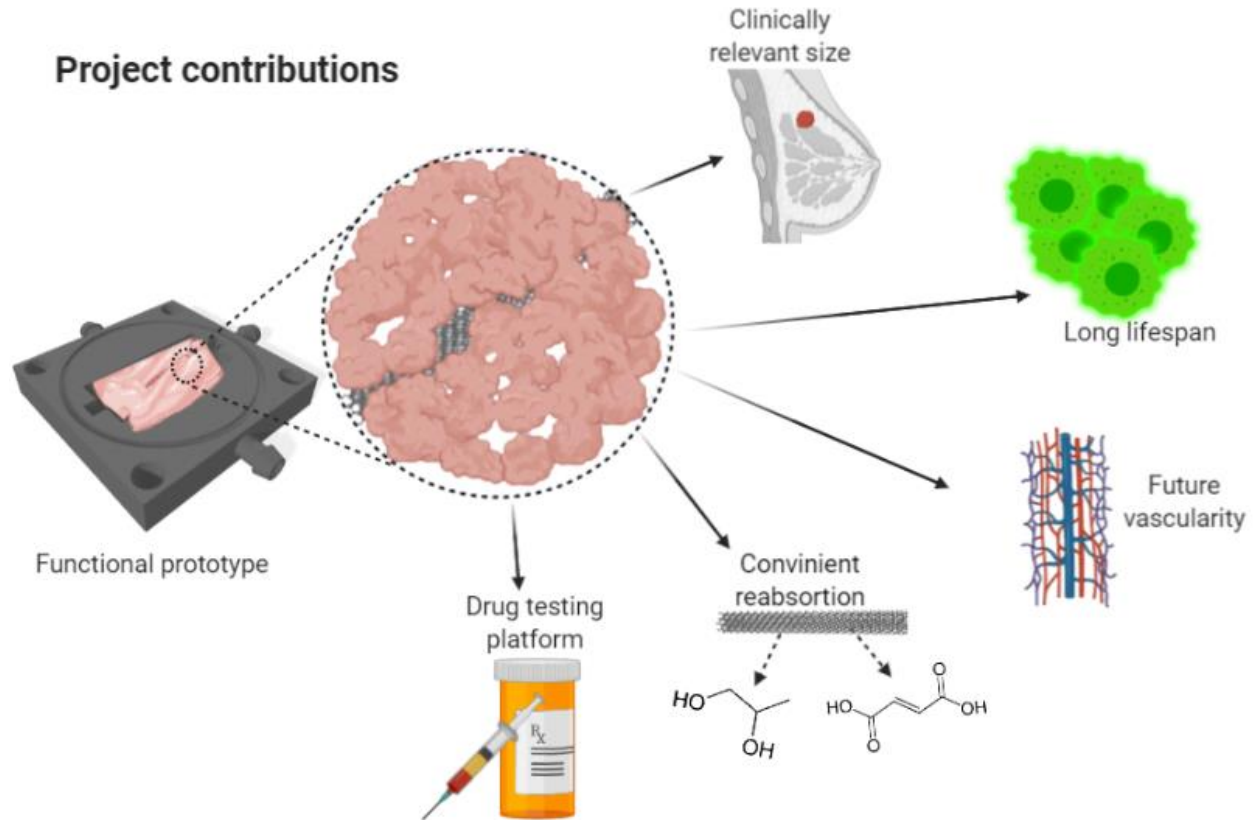
This document provides a viable and working direct perfusion bioreactor developed using affordable and commercially available pieces with an adjustable control system and the ability of working inside an incubator. The flow rate profile found show promises of significant improvement in cell survival and differentiation than cell growing under static culture. the sheer stress cause by the flow is harmful for the cells. The scaffold's size and biodegradability, cell differentiation, viability and long lifespan obtained in this projects brings science a step closer to obtain cultured bone tissue of relevant size to be implanted substituting current treatments and diminishing the problems that it brings (Figure 23) . The authors propose a way of growing bone tissue in an absorbable material (PPF) scaffold with clinically relevant size for implantation, something that has not been able to achieve yet.



**Figure 23.**Key aspects for future successful implantation

The tumor-on-chip device designed and prototyped in this proposal has the potential of achieving size and a living time greater than what recent literature reports. This will be of great importance for drug testing and tumor's pathophysiology modeling. This design also gives the opportunity of monitoring and manipulating the tissue in study during its experimental phase. The central channel of the device forms part of another interesting feature as it is having a support less tumor tissue. Changing the material of the central channel, for example to PPF, provides the opportunity to have the featured describes earlier, as time passes and PPF is disintegrated and discarded in media, the support system will vanish and tumor tissue will stand alone.

Even though cellular characterization is still pending, the design process and printing facilities that DLP bring with it, provides the ability to change and restructure the design in case it is needed. Having this feature can save a lot of time and money and test different designs in a relatively short period of time. Figure 24 provides the summary of contributions this project brought and some other future applications and tests that could be done to increase the fidelity of the model proposed.



**Figure 24. Breast tumor-on-chip contributions**

Two bioreactors were designed and functionally prototyped during these projects. The incorporation of design, printing, prototyping, and validation techniques were a key aspect that tie both projects together. The experience developed during the advancement of the perfusion bioreactor project gave the authors the capacity of integrating design and fabrication methods to create a functional prototype of the tumor-on-chip device.

Both prototypes provide the opportunity of creating tissue of greater magnitude level than what is stated in current literature. The incorporation of flow and perfusion channels will also maintain created tissue alive for an extended period of time (1-2 months). Cost-effectiveness was also optimized using DLP printing technique as well as using commercially available parts.

Even though cell culture experimentation was not performed due to COVID-19 confinement issues, all the experimental plan is clearly stated in this document and ready to be implemented. Expected results provide an insight of the behavior cell will present in the systems being evaluated, with visual representations that could help whoever will perform the experimentation. Literature review provides the basis for the speculated results, so the adaptation of the parameters used will come while experimenting.



## 5 References

- Agarwal, P., Wang, H., Sun, M., Xu, J., Zhao, S., Liu, Z., ... He, X. (2017). Microfluidics Enabled Bottom-Up Engineering of 3D Vascularized Tumor for Drug Discovery HHS Public Access, *11*(7), 6691–6702. <https://doi.org/10.1021/acsnano.7b00824>
- Amini, A., Laurencin, C., & Nukavarapu, S. (2012). Bone tissue engineering: Recent advances and challenges. *Critical Reviews in Biomedical Engineering*, *40*(5), 363–408. <https://doi.org/10.1615/CritRevBiomedEng.v40.i5.10>
- Arano, T., Sato, T., Matsuzaka, K., Ikada, Y., & Yoshinari, M. (2010). Osteoblastic Cell Proliferation with Uniform Distribution in a Large Scaffold Using Radial-Flow Bioreactor. *Tissue Engineering Part C: Methods*, *16*(6), 1387–1398. <https://doi.org/10.1089/ten.tec.2009.0377>
- Bashraheel, S. S., Domling, A., & Goda, S. K. (2020, May 1). Update on targeted cancer therapies, single or in combination, and their fine tuning for precision medicine. *Biomedicine and Pharmacotherapy*. Elsevier Masson SAS. <https://doi.org/10.1016/j.biopha.2020.110009>
- Behrens, M. R., Fuller, H. C., Swist, E. R., Wu, J., Long, Z., Ruder, W. C., & Steward, R. (2020). Open-source, 3D-printed Peristaltic Pumps for Small Volume Point-of-Care Liquid Handling. <https://doi.org/10.1038/s41598-020-58246-6>
- Chen, Y., Gao, D., Wang, Y., Lin, S., & Jiang, Y. (2018). A novel 3D breast-cancer-on-chip platform for therapeutic evaluation of drug delivery systems. *Analytica Chimica Acta*, *1036*, 97–106. <https://doi.org/10.1016/j.aca.2018.06.038>
- De Luca, A., Vitrano, I., Costa, V., Raimondi, L., Carina, V., Bellavia, D., ... Giavaresi, G. (2020). Improvement of osteogenic differentiation of human mesenchymal stem cells on composite poly L-lactic acid/nano-hydroxyapatite scaffolds for bone defect repair. *Journal of Bioscience and Bioengineering*, *129*(2), 250–257. <https://doi.org/10.1016/j.jbiosc.2019.08.001>
- Friedrich, J., Seidel, C., Ebner, R., & Kunz-Schughart, L. A. (2009). Spheroid-based drug screen: Considerations and practical approach. *Nature Protocols*, *4*(3), 309–324. <https://doi.org/10.1038/nprot.2008.226>
- Hanahan, D., & Weinberg, R. A. (2011, March 4). Hallmarks of cancer: The next generation. *Cell*. Cell Press. <https://doi.org/10.1016/j.cell.2011.02.013>
- Heylman, C., Sobrino, A., Shirure, V. S., Hughes, C. C. W., & George, S. C. (2014). A strategy for integrating essential 3D microphysiological systems of human organs for realistic anti-cancer drug screening. *Exp Biol Med (Maywood)*. <https://doi.org/10.1177/1535370214525295>
- Hutmacher, D. W. (2000). Scaffolds in tissue engineering bone and cartilage. In *The Biomaterials: Silver Jubilee Compendium* (pp. 175–189). Elsevier Ltd. <https://doi.org/10.1016/B978-008045154-1.50021-6>
- Kanda, Y., Nishimura, I., Sato, T., Katayama, A., Arano, T., Ikada, Y., & Yoshinari, M. (2016). Dynamic cultivation with radial flow bioreactor enhances proliferation or differentiation of rat bone marrow cells by fibroblast growth factor or osteogenic differentiation factor. *Regenerative Therapy*, *5*, 17–24. <https://doi.org/10.1016/j.reth.2016.06.001>
- Kheirallah, M., & Almeshaly, H. (2016). Present Strategies for Critical Bone Defects Regeneration. <https://doi.org/10.4172/2471-8726.1000127>
- Kim, C., Yang, J., Cho, H., Lee, B. S., Mok Gwon, T., Shin, S., ... Hwang, S. J. (2019). Implantable electrical stimulation bioreactor with liquid crystal polymer based electrodes for enhanced bone regeneration at mandibular large defects in rabbit. *Medical & Biological Engineering & Computing*, *58*. <https://doi.org/10.1101/402719>



- Kleinhans, C., Mohan, R. R., Vacun, G., Schwarz, T., Haller, B., Sun, Y., ... Hansmann, J. (2015). A perfusion bioreactor system efficiently generates cell-loaded bone substitute materials for addressing critical size bone defects. *Biotechnology Journal*, 10(11), 1727–1738. <https://doi.org/10.1002/biot.201400813>
- Kwak, B., Ozcelikkale, A., Shin, C. S., Park, K., & Han, B. (2014). Simulation of Complex Transport of Nanoparticles around a Tumor Using Tumor-Microenvironment-on-Chip. *J Control Release*, 194, 157–167. <https://doi.org/10.1016/j.jconrel.2014.08.027>
- Lim, K. T., Patel, D. K., Seonwoo, H., Kim, J., & Chung, J. H. (2019). A fully automated bioreactor system for precise control of stem cell proliferation and differentiation. *Biochemical Engineering Journal*, 150, 107258. <https://doi.org/10.1016/j.bej.2019.107258>
- Lim, W., & Park, S. (2018). A microfluidic spheroid culture device with a concentration gradient generator for high-throughput screening of drug efficacy. *Molecules*, 23(12), 3355. <https://doi.org/10.3390/molecules23123355>
- Lovecchio, J., Gargiulo, P., Luis Vargas Luna, J., Giordano, E., & eysteinn Sigurjónsson, Ó. (2019). A standalone bioreactor system to deliver compressive load under perfusion flow to hBMSC-seeded 3D chitosan-graphene templates. *Scientific Reports*, 9. <https://doi.org/10.1038/s41598-019-53319-7>
- Luo, Y., Dolder, C. K., Walker, J. M., Mishra, R., Dean, D., & Becker, M. L. (2016). Synthesis and Biological Evaluation of Well-Defined Poly(propylene fumarate) Oligomers and Their Use in 3D Printed Scaffolds. *Biomacromolecules*, 17(2), 690–697. <https://doi.org/10.1021/acs.biomac.6b00014>
- Mannino, R. G., Pradhan, P., Roy, K., & Lam, W. A. (2018). 3D in vitro microvascular model-based lymphoma model. In *Methods in Cell Biology* (Vol. 146, pp. 149–158). Academic Press Inc. <https://doi.org/10.1016/bs.mcb.2018.05.007>
- Meng, F., Meyer, C. M., Joung, D., Vallera, D. A., Mcalpine, M. C., & Panoskaltsis-Mortari, A. (2019). 3D Bioprinted In Vitro Metastatic Models via Reconstruction of Tumor Microenvironments HHS Public Access. *Advanced Materials*. <https://doi.org/10.1002/adma.201806899>
- Michna, R., Gadde, M., Ozkan, A., Dewitt, ; Matthew, Rylander, M., Dean, E., & St, K. (2018). Vascularized Microfluidic Platforms to Mimic the Tumor Microenvironment. *Biotechnology & Bioengineering*, 115(11), 2793–2806. <https://doi.org/10.1002/bit.26778>
- Mishra, R., Sefcik, R. S., Bishop, T. J., Montelone, S. M., Crouser, N., Welter, J. F., ... Dean, D. (2016). Growth Factor Dose Tuning for Bone Progenitor Cell Proliferation and Differentiation on Resorbable Poly(propylene fumarate) Scaffolds. *Tissue Engineering Part C: Methods*, 22(9), 904–913. <https://doi.org/10.1089/ten.tec.2016.0094>
- Moultrie, J. (n.d.). Morphological charts. Retrieved May 4, 2020, from <https://www.ifm.eng.cam.ac.uk/research/dmg/tools-and-techniques/morphological-charts/>
- Nashimoto, Y., Okada, R., Hanada, S., Arima, Y., Nishiyama, K., Miura, T., & Yokokawa, R. (2020). Vascularized cancer on a chip: The effect of perfusion on growth and drug delivery of tumor spheroid. *Biomaterials*, 229. <https://doi.org/10.1016/j.biomaterials.2019.119547>
- Nokhbatolfoghahaei, H., Bohlouli, M., Paknejad, Z., R. Rad, M., M. Amirabad, L., Salehi-Nik, N., ... Khojasteh, A. (2020). Bioreactor cultivation condition for engineered bone tissue: Effect of various bioreactor designs on extra cellular matrix synthesis. *Journal of Biomedical Materials Research - Part A*. <https://doi.org/10.1002/jbm.a.36932>
- Orlando, G. (2014). *Regenerative Medicine Applications in Organ Transplantation. Regenerative Medicine Applications in Organ Transplantation*. Elsevier Inc. <https://doi.org/10.1016/C2012-0-00629-1>
- Paek, J., Park, S. E., Lu, Q., Park, K.-T., Cho, M., Oh, J. M., ... Huh, D. (2019). Microphysiological Engineering of Self-Assembled and Perfusable Microvascular Beds for the Production of Vascularized Three-Dimensional Human Microtissues. *ACS Nano*, 13(7), 7627–7643. <https://doi.org/10.1021/acsnano.9b00686>
- Pradhan, S., Smith, A. M., Garson, C. J., Hassani, I., Seeto, W. J., Pant, K., ... Lipke, E. A. (2018). A

- Microvascularized Tumor-mimetic Platform for Assessing Anti-cancer Drug Efficacy OPEN. *SCienTific RePoRTS* |, 8, 3171. <https://doi.org/10.1038/s41598-018-21075-9>
- Rasheed, T., Li, C., Nabeel, F., Qi, M., Zhang, Y., & Yu, C. (2018). Real-time probing of mercury using an efficient “turn-on” strategy with potential as in-field mapping kit and in live cell imaging. *New Journal of Chemistry*, 42(13), 10940–10946. <https://doi.org/10.1039/c8nj01746h>
- Rodrigues, T., Kundu, B., Silva-Correia, J., Kundu, S. C., Oliveira, J. M., Reis, R. L., & Correlo, V. M. (2018, April 1). Emerging tumor spheroids technologies for 3D in vitro cancer modeling. *Pharmacology and Therapeutics*. Elsevier Inc. <https://doi.org/10.1016/j.pharmthera.2017.10.018>
- Rodriguez, C. A., Lara-Padilla, H., & Dean, D. (2018). *Bioceramics for Musculoskeletal Regenerative Medicine: Materials and Manufacturing Process Compatibility for Synthetic Bone Grafts and Medical Devices*. *3D Printing and Biofabrication*. [https://doi.org/10.1007/978-3-319-45444-3\\_22](https://doi.org/10.1007/978-3-319-45444-3_22)
- Santoro, M., Lamhamedi-Cherradi, S. E., Menegaz, B. A., Ludwig, J. A., & Mikos, A. G. (2015). Flow perfusion effects on three-dimensional culture and drug sensitivity of Ewing sarcoma. *Proceedings of the National Academy of Sciences of the United States of America*, 112(33), 10304–10309. <https://doi.org/10.1073/pnas.1506684112>
- Sauerova, P., Suchy, T., Supova, M., Bartos, M., Klima, J., Juhasova, J., ... Hubalek Kalbacova, M. (2019). Positive impact of dynamic seeding of mesenchymal stem cells on bone-like biodegradable scaffolds with increased content of calcium phosphate nanoparticles. *Molecular Biology Reports*, 46(4), 4483–4500. <https://doi.org/10.1007/s11033-019-04903-7>
- Shalumon, K. T., Liao, H. T., Kuo, C. Y., Wong, C. B., Li, C. J., Mini, P. A., & Chen, J. P. (2019). Rational design of gelatin/nanohydroxyapatite cryogel scaffolds for bone regeneration by introducing chemical and physical cues to enhance osteogenesis of bone marrow mesenchymal stem cells. *Materials Science and Engineering C*, 104, 109855. <https://doi.org/10.1016/j.msec.2019.109855>
- Shirure, V. S., Bi, Y., Curtis, M. B., Lezia, A., Goedegebuure, M. M., Goedegebuure, S. P., ... George, S. C. (2018). Tumor-on-a-chip platform to investigate progression and drug sensitivity in cell lines and patient-derived organoids. *Lab on a Chip*, 18(23), 3687–3702. <https://doi.org/10.1039/c8lc00596f>
- Singh, M., Mukundan, S., Jaramillo, M., Oesterreich, S., & Sant, S. (2016). Three-Dimensional Breast Cancer Models Mimic Hallmarks of Size-Induced Tumor Progression. <https://doi.org/10.1158/0008-5472.CAN-15-2304>
- Sobrinho, A., Phan, D. T. T., Datta, R., Wang, X., Hachey, S. J., Romero-López, M., ... Hughes, C. C. W. (2016). 3D microtumors in vitro supported by perfused vascular networks. *Nature Publishing Group*. <https://doi.org/10.1038/srep31589>
- Stoodley, P., DeBeer, D., & Lewandowski, Z. (1994). Liquid flow in biofilm systems. *Applied and Environmental Microbiology*, 60(8), 2711–2716. <https://doi.org/10.1128/aem.60.8.2711-2716.1994>
- Trujillo-de Santiago, G., Flores-Garza, B. G., Tavares-Negrete, J. A., Lara-Mayorga, I. M., González-Gamboa, I., Zhang, Y. S., ... Álvarez, M. M. (2019, September 1). The tumor-on-chip: Recent advances in the development of microfluidic systems to recapitulate the physiology of solid tumors. *Materials*. MDPI AG. <https://doi.org/10.3390/ma12182945>
- Uygun, B. E., Uygun, K., & Yarmush, M. (2011, October 1). Liver tissue engineering. Elsevier.
- Vetsch, J. R., Betts, D. C., Mü Ller, R., & Hofmann, S. (2017). Flow velocity-driven differentiation of human mesenchymal stromal cells in silk fibroin scaffolds: A combined experimental and computational approach. <https://doi.org/10.1371/journal.pone.0180781>
- Volkmer, E., Drosse, I., Otto, S., Stangelmayer, A., Stengele, M., Kallukalam, B. C., ... Schieker, M. (2008a). Hypoxia in static and dynamic 3D culture systems for tissue engineering of bone. *Tissue Engineering - Part A*, 14(8), 1331–1340. <https://doi.org/10.1089/ten.tea.2007.0231>
- Volkmer, E., Drosse, I., Otto, S., Stangelmayer, A., Stengele, M., Kallukalam, B. C., ... Schieker, M. (2008b). Hypoxia in Static and Dynamic 3D Culture Systems for Tissue Engineering of Bone. *Tissue Engineering Part A*, 14(8), 1331–1340. <https://doi.org/10.1089/ten.tea.2007.0231>

- Walker, J. M., Bodamer, E., Kleinfehn, A., Luo, Y., Becker, M. L., & Dean, D. (2017). Design and mechanical characterization of solid and highly porous 3D printed poly(propylene fumarate) scaffolds, 2, 99–108. <https://doi.org/10.1007/s40964-017-0021-3>
- Walker, J. M., Bodamer, E., Krebs, O., Luo, Y., Kleinfehn, A., Becker, M. L., & Dean, D. (2017). Effect of Chemical and Physical Properties on the In Vitro Degradation of 3D Printed High Resolution Poly(propylene fumarate) Scaffolds. *Biomacromolecules*, 18(4), 1419–1425. <https://doi.org/10.1021/acs.biomac.7b00146>
- Wang, Shanfeng, Lu, L., & Yaszemski, M. J. (2006). Bone-tissue-engineering material poly(propylene fumarate): Correlation between molecular weight, chain dimension, and physical properties. *Biomacromolecules*, 7(6), 1976–1982. <https://doi.org/10.1021/bm060096a>
- Wang, Shuang, He, Y.-F., Ma, J., Yu, L., Wen, J.-K., & Ye, X.-J. (2020). Dynamic Bioreactor Culture for Infiltration of Bone Mesenchymal Stem Cells within Electrospun Nanofibrous Scaffolds for Annulus Fibrosus Repair. <https://doi.org/10.1111/os.12615>
- Weiswald, L. B., Bellet, D., & Dangles-Marie, V. (2015, January 1). Spherical Cancer Models in Tumor Biology. *Neoplasia (United States)*. Neoplasia Press, Inc. <https://doi.org/10.1016/j.neo.2014.12.004>
- WHO. (2018). Cancer. Retrieved May 31, 2020, from <https://www.who.int/news-room/fact-sheets/detail/cancer>
- Yaghoobi, M., Hashemi-Najafabadi, S., Soleimani, M., & Vasheghani-Farahani, E. (2019). Osteogenic induction of human mesenchymal stem cells in multilayered electrospun scaffolds at different flow rates and configurations in a perfusion bioreactor. *Journal of Bioscience and Bioengineering*, 128(4), 495–503. <https://doi.org/10.1016/j.jbiosc.2019.03.015>
- Yeatts, A. B., & Fisher, J. P. (2011, February 1). Bone tissue engineering bioreactors: Dynamic culture and the influence of shear stress. *Bone*. Elsevier. <https://doi.org/10.1016/j.bone.2010.09.138>
- Zhang, Z.-Y., Teoh, H., Teo, E. Y., Seow, M., Chong, K., Shin, C. W., ... Chan, J. K. Y. (2010). A comparison of bioreactors for culture of fetal mesenchymal stem cells for bone tissue engineering. *Biomaterials*, 31. <https://doi.org/10.1016/j.biomaterials.2010.07.097>

## 6 Appendix A. PPF Chemical Structure

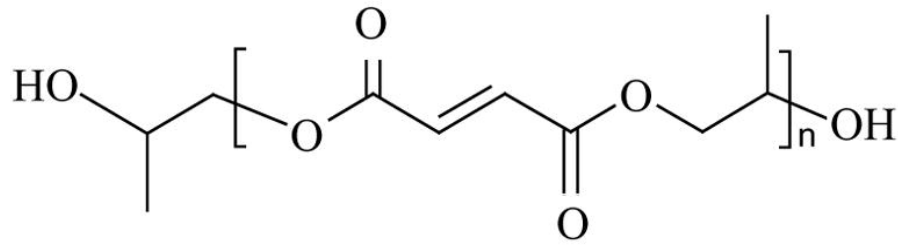


Figure 1A. Chemical structure of PPF (Shanfeng Wang et al., 2006)

## 7 Appendix B. Necrotic Core Visual Aids

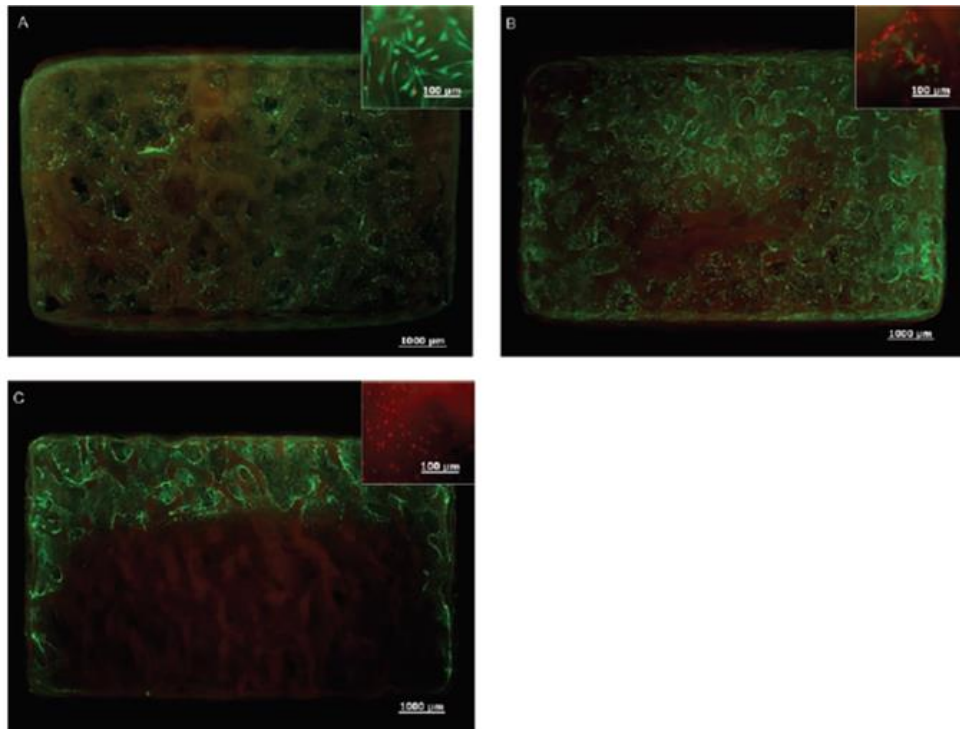
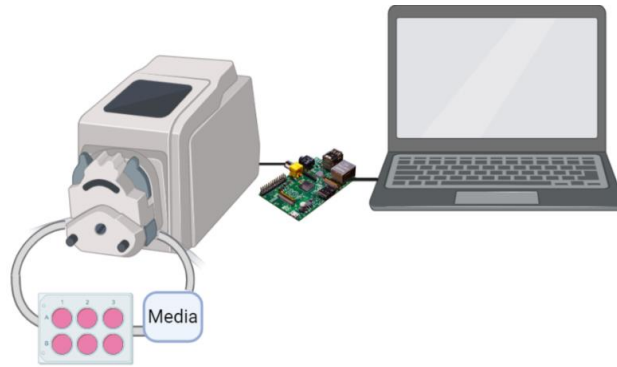


Figure 1B. Live-dead assay (Volkmer et al., 2008a)

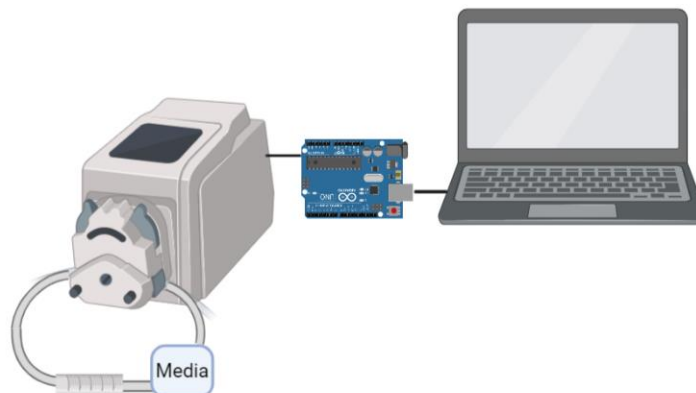
## 8 Appendix C. Sketches Made with the Morphological Matrix



**Figure 1C.** Combination number 1. It integrates the roller peristaltic pump, RaspberryPi control system and six-well plate as incubation chamber.



**Figure 2C.** Combination number 2. It integrates the syringe pump, DAQ internal control system and glass syringe as incubation chamber



**Figure 3C.** Combination number 3. It integrates the roller peristaltic pump, Arduino control system and plastic syringe as incubation chamber.

**Figure 4C.** Combination number 4. It integrates the linear peristaltic pump, DAQ control system and 3D printed incubation chamber.

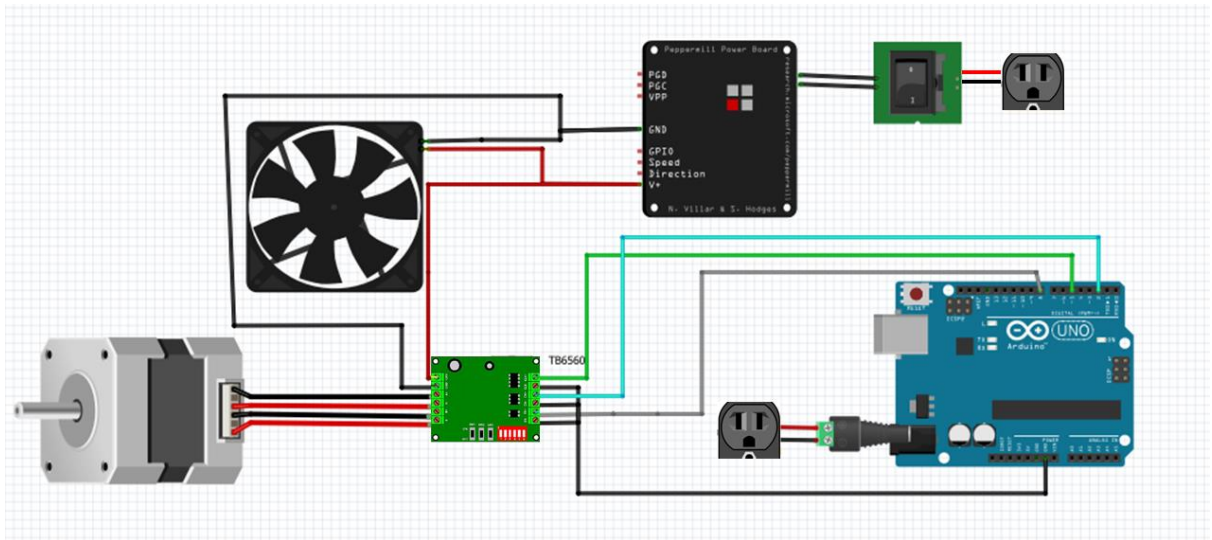
9 Appendix D. DG4 Multi-channel Head® by Chongqing Jieheng Peristaltic Pump Co., Ltd®



**Figure1D.** DG4 Multi-channel Head® by Chongqing Jieheng Peristaltic Pump Co., Ltd®

This model has the option of expanding the lines using only one motor by stacking head pumps one in front of the other and coupling them. This provides the opportunity of running multiple lines for large experiments at the same time with only one control system.

## 10 Appendix E. Electric circuit of peristaltic pump and Arduino code

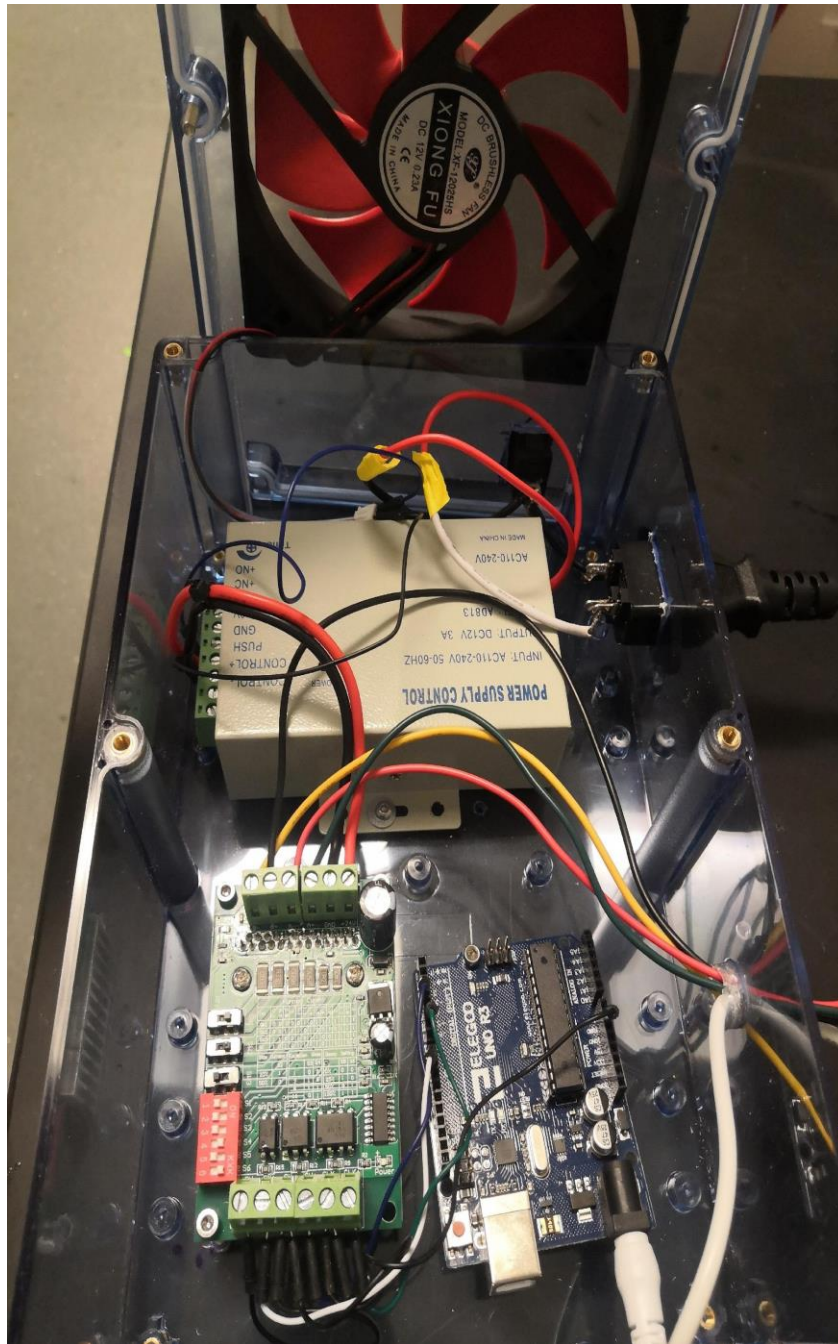


**Figure 1E.** Electric schematic of the perfusion pump's control system

To get the electric current the motor needs the configuration of the switches in the Stepper Motor Driver should be the following.

SW1	SW2	SW3	S1	S2	S3	S4	S5	S6
ON	ON	OFF	OFF	OFF	OFF	ON	OFF	ON





**Figure 2E.** Electric connections in the box

Arduino code that runs the pump

```
// defines pins numbers
const int stepPin = 5;
const int dirPin = 2;
const int enPin = 8;
const int Up = 4;
```



```

const int Down = 7;

int Pause = 15000; // Max pause, a bigger number will mess up the system

void setup() {

  // Sets the two pins as Outputs
  pinMode(stepPin,OUTPUT);
  pinMode(dirPin,OUTPUT);
  pinMode(enPin,OUTPUT);
  pinMode(Up,INPUT);
  pinMode(Down,INPUT);
  digitalWrite(enPin,LOW);// turn on motor

}

void loop() {

  digitalWrite(dirPin,LOW); // Enables the motor to move in a particular direction
  for(int x = 0; x < 800; x++)
  {
    digitalWrite(stepPin,HIGH);
    delayMicroseconds(Pause);
    digitalWrite(stepPin,LOW);
    delayMicroseconds(Pause);
  }
}

```

## 11 Appendix F. DLP printing process

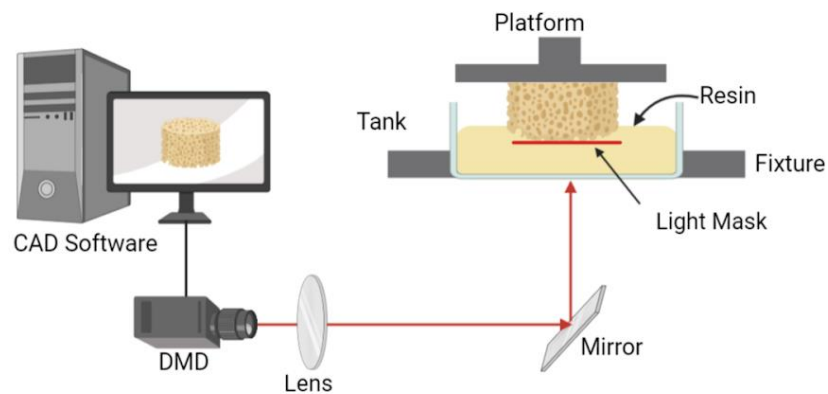


Figure 1.F. DLP Printing process

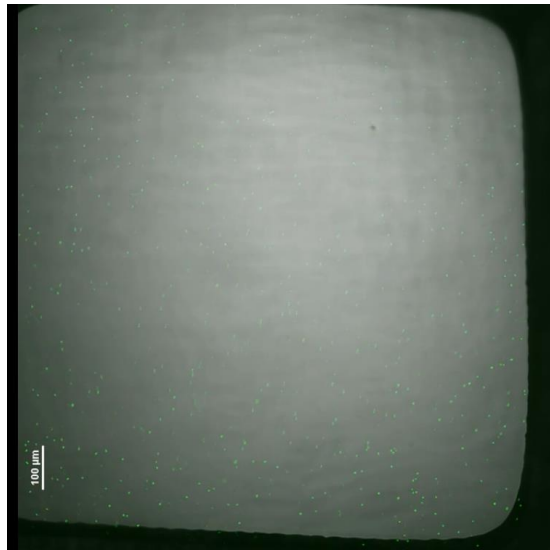
## 12 Appendix G. CFD and Particle Tracking Video Analysis



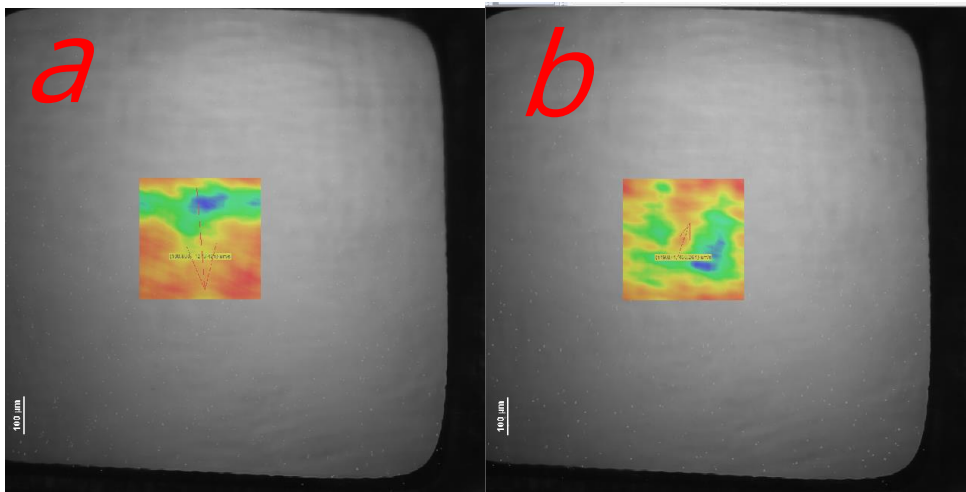
Particle Study.avi



Flow  
Trajectories.avi



**Figure 1G.** Pore showing fluorescent particles



**Figure 2G.** Velocity vectors showing  $Q_f$  (a) and  $Q_b$  (b).

	Right	Center	Left	Total Average Velocity (um/s)				
Forward	1141.84924	1079.5321	932.335268	1051.23887				
Backwards	898.522886	976.651361	797.15165	890.775299				
	Average For	Average Bac						
LeftInfCor	1386.37205	1142.10535			1 cycle (11 Seg)			
LeftCenter	995.954635	860.905752			Forward (8seg)	Backwards (3seg)	Total Displacemnt total(um)	
LeftInfCor	1043.22104	762.285835			8409.910956	2672.325897	5737.585059	
CenterSup	805.852001	833.781599	11 ml/hr	Q=Av	Experimental data			
Center	1285.89278	1234.54627		Chamber	Average Velocity (m/s)			
CenterInf	1146.85152	861.62621		Tubes	0.000041778			
RightInfCor	952.677494	894.962796		Average	0.00097261			
RightCenter	1179.11748	866.218365			Displacement 1 min			
RightSupCor	665.210826	630.27379			um		m	
					31295.91851	0.031295919	5.22E-04	
					Velocity in Video (m/s)			
					521.5986418			
					1.44E-05			
					2.761633296			
					Velocity (m/s)			
					Flow Test 0.000507194			
					Microfluidic Device 0.000521599			

$$1) \text{ Pipe Diameter} = \sqrt{\frac{4 \cdot \text{flow rate}}{\pi \cdot \text{velocity}}}$$

$$2) \text{ Velocity} = \frac{4 \cdot \text{flow rate}}{\pi \cdot (\text{pipe diameter})^2}$$

$$3) \text{ Flow Rate} = \frac{1}{4} \cdot \pi \cdot (\text{pipe diameter})^2 \cdot \text{velocity}$$

Velocity (m/s)	
Flow Test	0.000507194
Microfluidic Device	0.000521599

Figure 3G. Excel sheet with calculations for  $VQ_f$ ,  $VQ_b$  and average flow rate.

### 13 Appendix H. PureLink® RNA Mini Kit protocol

[https://assets.thermofisher.com/TFS-Assets/LSG/manuals/purelink\\_rna\\_mini\\_kit\\_man.pdf](https://assets.thermofisher.com/TFS-Assets/LSG/manuals/purelink_rna_mini_kit_man.pdf)